Available online at www.sciencedirect.com
SCIENCE DIRECT®
Chemical Physics 319 (2005) 69–92
Chemical Physics
www.elsevier.com/locate/chemphys

Dynamic NMR studies of base-catalyzed intramolecular single vs. intermolecular double proton transfer of 1,3-bis(4-fluorophenyl)triazene

Hans-Heinrich Limbach [a,*], Ferdinand Männle [a,1], Carsten Detering [a,2], Gleb S. Denisov [b]

[a] Institut für Chemie der Freien Universität Berlin, Takustrasse 3, D-14195 Berlin, Germany
[b] Institute of Physics, St. Petersburg State University, 198504 St. Petersburg, Russian Federation

Received 4 May 2005; accepted 10 May 2005
Available online 3 August 2005

Abstract

In this paper, we explore the mechanisms of degenerate base-catalyzed intra- and intermolecular proton transfer using dynamic liquid state NMR. For this purpose, the model compound 1,3-bis(4-fluorophenyl)[1,3-$^{15}N_2$]triazene (**1**) was studied with and without the presence of dimethylamine (**2**), trimethylamine (**3**) and water, using tetrahydrofuran-d_8 and methylethylether-d_8 as solvents, down to 130 K. Compound **1** represents an analog of carboxylic acids and of diarylamidines forming cyclic dimers in which a fast double proton transfer takes place. By contrast, the structure of **1** was chosen in such a way that this double proton transfer is suppressed, thus revealing the base catalyzed transfer by dynamic ^{1}H and ^{19}F NMR. Surprisingly, both **2** and **3** can pick up the mobile proton of **1** at one nitrogen atom and carry it to the other nitrogen atom of **1**, resulting in an intramolecular transfer process catalyzed each time by a different base molecule. Even more surprising is that the intramolecular transfer catalyzed by **2** is faster than the superimposed intermolecular double proton transfer. In the absence of added bases, a **1** is subject to a slow proton exchange with 2-amino-5,4′-difluoro-diphenyl-diazene (**4**) which is formed in small quantities from **1** in the presence of acid impurities. This process can be minimized by a proper sample preparation technique.

The kinetic H/D isotope effects are small, especially in the catalysis by **2**, indicating a major heavy atom rearrangement and absence of tunneling. Semi-empirical PM3 and ab initio DFT calculations indicate a reaction pathway via a hydrogen bond switch of the protonated amine representing the transition state. The Arrhenius curves of all processes exhibit strong convex curvatures. This phenomenon is explained in terms of the hydrogen bond association of **1** with the added bases, preceding the proton transfer. At low temperatures, all catalysts are in a hydrogen bonded reactive complex with **1**, and the rate constants observed equal to those of the reacting complex. However, at high temperatures, dissociation of the complex occurs, and the temperature dependence of the observed rate constants is affected also by the enthalpy of the hydrogen bond association. Finally, implications of this study for the mechanisms of enzyme proton transfers are discussed.

1. Introduction

Functional groups of amino acid side chains such as COOH-groups, histidine or lysine groups of proteins are often involved in various types of acid–base catalyzed reactions by assisting the transfer of protons from one molecular site to another [1–3]. In order to understand these often very complex reaction pathways, chemical reaction models have been studied where a bifunctional

* Corresponding author. Tel.: +49 30 838 5375; fax: +49 30 838 5310.
E-mail address: limbach@chemie.fu-berlin.de (H.-H. Limbach).
[1] Present address: SINTEF Materialteknologi, Forskningsveien 1, N-0314 Oslo.
[2] Present address: University of Washington, Department of Chemistry, Seattle, WA 91895-1700, USA.

0301-0104/$ - see front matter © 2005 Published by Elsevier B.V.
doi:10.1016/j.chemphys.2005.05.021

catalyst can take up a proton from one site of a substrate and release another proton to a second site [4,5]. The mechanisms of double and multiple proton and deuteron transfer reactions alone have also been studied in cyclic dimers of carboxylic acids (Scheme 1a) [6], between acetic acid and methanol [7], pyrazoles [8], and *N*,*N*-diarylamidines (Scheme 1b) [9], which are the nitrogen analogs of carboxylic acids. Bifunctional basic amidines have been studied by Ahlberg and others [5] as catalysts for 1,3-proton shifts of the type $R–CH_2–X{=}CR_2 \rightarrow R–CH{=}X–CHR_2$, where in particular the problem of a concerted vs. a stepwise proton transfer was addressed. In nature, the key step of transaminase reactions involves a similar reaction with X = N, and the lysine terminal amino group as base catalyst [2,4e,4f,5d].

The goal of this study was to explore the pathways of bifunctional base-catalyzed proton transfer by dynamic NMR spectroscopy in further detail. Since the latter method requires degenerate or at least quasi-degenerate reactions, we have been looking for model compounds exhibiting two chemically equivalent proton binding sites, but which are not able to form cyclic hydrogen bonded intermediates exhibiting very fast double proton transfer which masks the base catalyzed transfer processes. This is, for example, the case in carboxylic acids [6] and amidines [9] (Scheme 1).

In order to find the desired chemical model we started from our previous work on 1,3-bis(4-fluorophenyl)amidine-$^{15}N_2$ (Scheme 1b). The fluorine and ^{15}N labels had made it possible to measure the full kinetic HH/HD/DD-isotope effects by dynamic NMR using tetrahydrofuran-d_8 as solvent. As found by X-ray crystallography and solid state NMR [9d], due to a steric interaction between the aromatic protons and the amidine CH-proton, the aryl rings are not coplanar with the amidine unit. When the aryl twist angles are unfavorable, the symmetry of the double proton transfer potential is lifted (Scheme 1b) [9d]. This finding incited us to study the analogous 1,3-bis(4-fluorophenyl)[1,3-$^{15}N_2$]triazene (**1**),

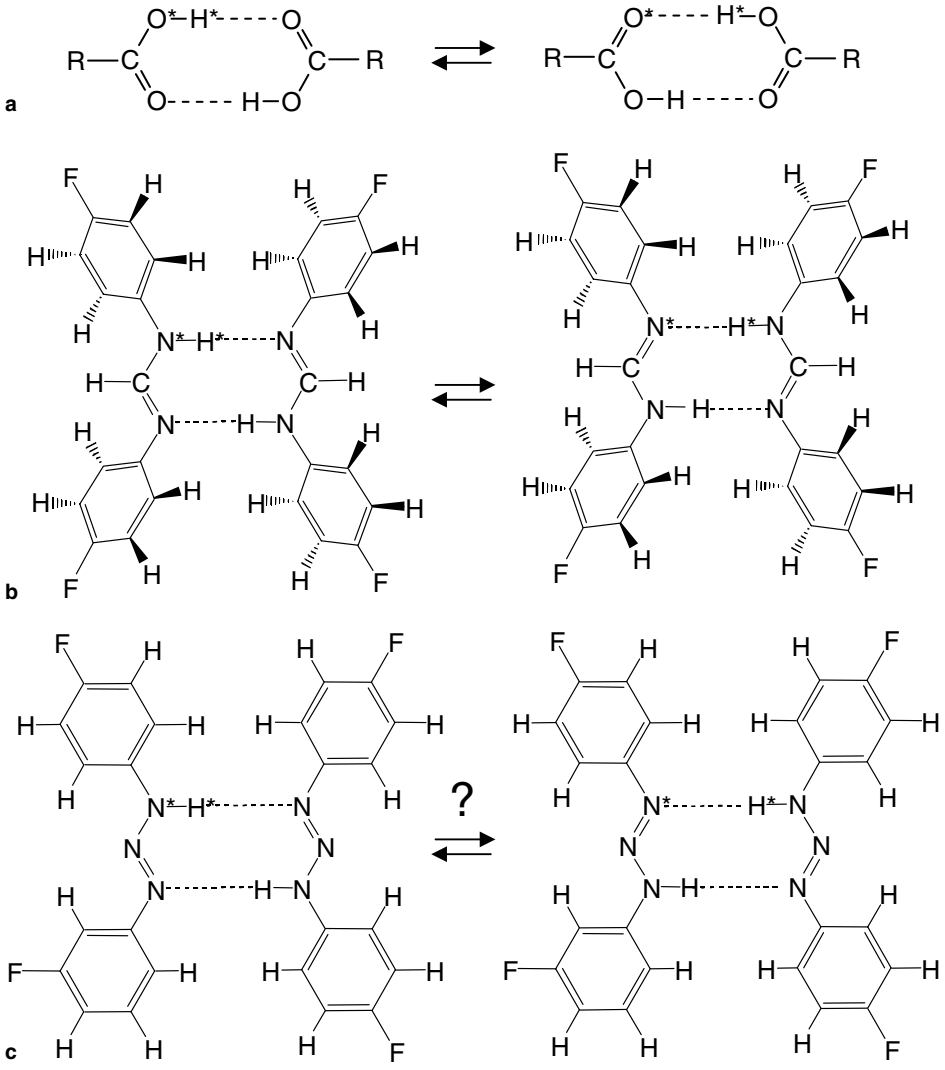

Scheme 1.

where the formyl CH-unit is replaced by a third nitrogen atom (Scheme 1c). We anticipated that the steric interaction between the aromatic proton and the central nitrogen atom is small so that the aryl groups are coplanar. This feature, however, should prevent the formation of cyclic dimers due to steric intermolecular interactions between the aromatic protons and hence suppress the double proton transfer as illustrated in Scheme 1c, opening the possibility to study the effects of added bases on the proton tautomerism of **1**. Indeed, in the solid state diaryltriazenes exhibit aryl groups which are coplanar with the triazene moieties, however, the molecules form linear hydrogen bonded chains in which intermolecular steric interactions are minimized [10].

The tautomerism of triazenes was first described by Nesmeyanov et al. [11]. A dynamic NMR study of Lunazzi et al. [12] revealed that the rate laws of the proton self-exchange processes of diaryltriazenes are either first order or second order with respect to the concentration of the triazene studied. This finding was associated to a reaction mechanism according to Scheme 2a, where in the first case the cyclic dimer and in the second the monomer is dominating.

Unfortunately, in the previous studies it was not recognized that diaryltriazenes such as **1** are subject to an acid catalyzed irreversible rearrangement to 2-aminodiaryl-diazenes such as **4** (Scheme 2) [13,14] which catalyzes the diaryltriazene proton exchange. In a first stage of this study of **1** in tetrahydrofuran-d_8, we found that indeed the apparent proton self-exchange of **1** can be substantially reduced by an improved sample preparation. We also could reproduce situations where this catalyzed exchange leads either to first- or to second-order reaction kinetics. Thus, we found that the mechanism of Scheme 2a is doubtful.

However, the positive side of this finding was that it opened also up the possibility to explore novel proton transfer pathways depicted in Scheme 2b and c, using added bases such as dimethylamine **2** and trimethylamine **3**. Using the latter, as the result of the ^{15}N labeling, we found evidence for the intramolecular proton transfer mechanism of Scheme 2b [15], where B carries the mobile proton of **1** from one binding site to the other, probably via a zwitterionic transition state. We anticipate that such a process also takes place with carboxylic acids or amidines, where it is, however, experimentally masked by the fast self-exchange. Normally, for a catalyst B containing a mobile proton one expects a transfer according Scheme 2c, consisting of the transfer of two protons in a stepwise or concerted fashion, without the requirement of major heavy atom motions. Pye et al. [16] have calculated the proton exchange of the parent

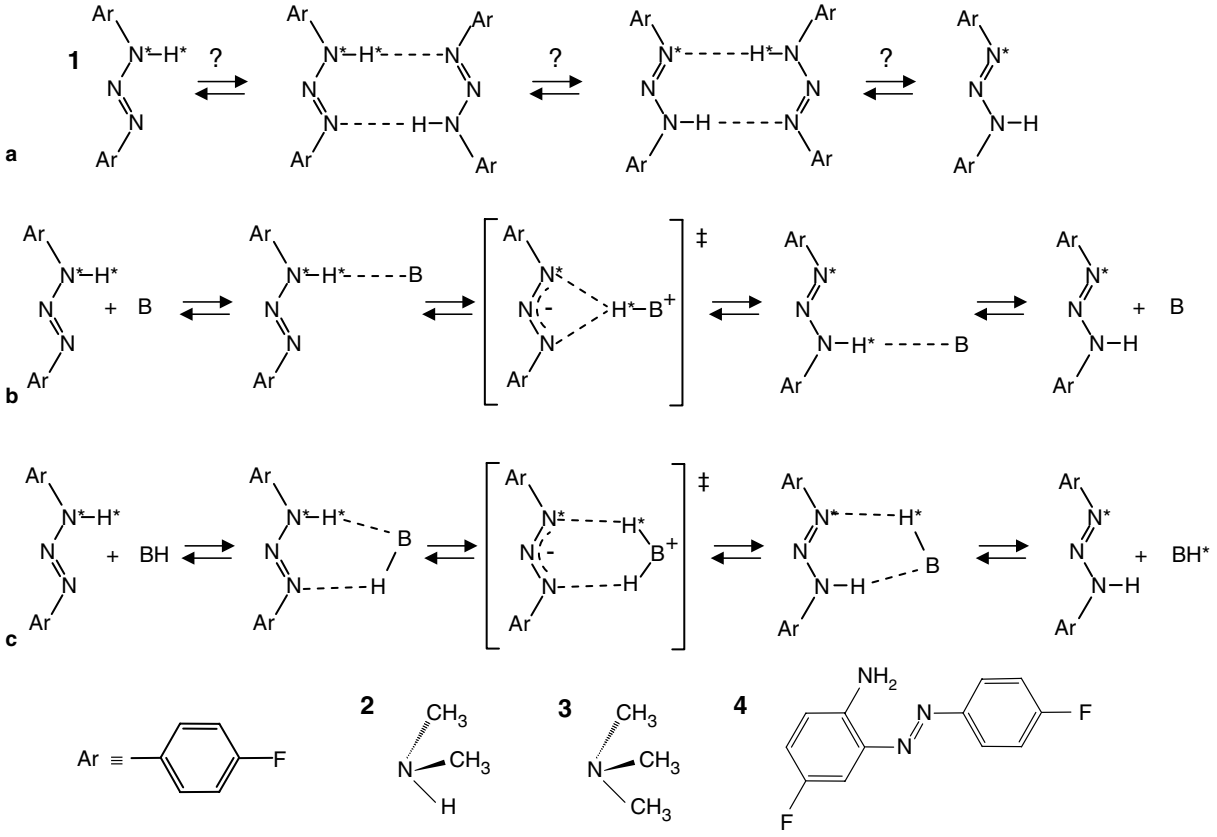

Scheme 2.

compound triazene with water using high-level ab initio calculations, and obtained evidence for a stepwise double proton mechanism where water protonates the triazene leading to a metastable intermediate [16]. On the other hand, for stronger bases one can conceive the contrary. Therefore, the question arises which pathway is preferred by a base such as **2** which requires major heavy atom rearrangements, in other words whether bifunctional catalysis is more efficient than monofunctional catalysis.

Because of this model character of the triazene-base tautomerism we have studied the exchange characteristics of **1** in the presence of water, **2** and **3** in more detail. The results of these experiments are reported in this paper. Whereas for the reaction with water tetrahydrofuran-d_8 could be employed, the reaction with the two latter bases required experiments at lower temperatures as can be achieved with this solvent. Therefore, we synthesized and employed here methylethylether-d_8, which is chemically close to tetrahydrofuran but which also allows measurements down to 130 K. During the experiments an interesting problem came up, leading to a temperature-dependent change of the rate law of the exchange: at low temperatures, the reacting complex dominates but dissociates at high temperatures into its components. This phenomenon leads to interesting convex Arrhenius curves. The occurrence of such curves has been found and discussed recently in the case of hydrogen transfer reactions in enzymes [17].

This paper is organized as follows. After an experimental part we describe in a theoretical section the influence of hydrogen bond complex formation on the proton exchange kinetics. Then, the results of the dynamic NMR spectroscopic experiments performed on **1** without and with water in tetrahydrofuran-d_8, and on **1** with **2** and **3** in methylethylether-d_8 are described, including kinetic H/D isotope effects. Some preliminary semi-empirical calculations of the intramolecular proton exchange of **1** catalyzed by **3** are presented. Finally, the results are discussed.

2. Experimental

2.1. Compounds

Compound **1** labeled in the N1, N3 positions with ^{15}N was prepared as follows. In a first step, *p*-F-substituted ^{15}N-benzamide was synthesized as reported previously [9c] from $^{15}NH_4Cl$ (95% ^{15}N, Chemotrade) and *p*-F-benzoyl chloride according to the method of Axenrod et al. [18]. The benzamide was then converted into *p*-F-aniline-^{15}N via Hofman degradation [9c,19]. The aniline was purified by vacuum transfer and converted into the hydrochloride by dissolving the reactant in dry ether and adding HCl gas. The product was recrystallized from *n*-hexane/ethanol (1:4). The triazene **1** was synthesized according to the procedure published for the non-labeled compound [20]. In order to minimize the formation of **4** (Scheme 2) [13] the synthesis of **1** was carried out under dry argon. In addition, all glassware which could come in contact with **1** was treated with a 5% solution of 1,4-dichloro-octamethyl-tetrasiloxane in hexane in order to remove surface OH-groups. Finally, the product was purified three times by chromatography under argon (aluminium oxide, toluene) followed by repeated recrystallisation from toluene (Fp. 118 °C).

Deuterated methylethylether $C_2D_5OCD_3$ as NMR solvent was prepared in an atmosphere of nitrogen as follows. 4.3 g (187 mmol) sodium was suspended in 40 ml (46.2 g, 696 mmol) ethanol-d_6. After the H_2 evolution was complete, 25 g (172 mmol) iodomethane-d_3 in ethanol-d_6 was added dropwise leading to the evolution of gaseous $C_2D_5OCD_3$ which was passed over solid KOH and condensed as a liquid using dry ice/acetone. Finally, the product (10.5 g, 90% yield) was condensed by vacuum transfer into a thick-wall glass container equipped with a needle valve and stored over anthracene–sodium–potassium alloy for removal of residual water and oxygen. The same procedure was used to purify THF-d_8 (Fluka).

Dimethylamine **2** and trimethylamine **3** were purchased from Merck (Darmstadt) and purified by distillation. Then they were placed in glass vessels and dried over freshly regenerated molecular sieve (4 Å, Merck).

2.2. Sample preparation

For the NMR experiments we used tubes equipped with teflon needle valves (Wilmad, Buena). Surface SiOH-groups in the inner glass walls of the NMR tubes were again removed before use by reaction with 1,4-dichloro-octamethyl-tetrasiloxane in hexane. Weighed amounts of **1** in toluene were placed under argon into an NMR tube which was then attached to a vacuum line, and the solvent removed in vacuo (12 h). The vacuum line was equipped with various calibrated tubes for the measurement of the volume of liquids in the μl to the ml range as described previously [21]. Desired amounts of dimethylamine **2** or trimethylamine **3** and about 0.5 ml of $C_2D_5OCD_3$ were transferred in vacuo from their corresponding container into the calibration tubes and then into the NMR tubes. The relative concentrations were later checked by ^1H NMR.

The deuterated samples were prepared as follows. Acid free CH_3OD (99%. Merck) was prepared by storage in different glass vessels over methanolate and then over molecular sieve (3 Å, Merck), which had been previously deuterated twice with D_2O and regenerated at 360 °C. The transfer of the solvent from one vessel to the other was performed in vacuo. Subsequently, 0.3 ml of CH_3OD were transferred into the NMR tube

filled with solid **1** and then removed. This procedure was carried out three times. Only then the bases and the solvent were added. In view of the small quantities of dimethylamine added, this compound was not deuterated before use.

2.3. NMR experiments

The NMR spectra were recorded on a Bruker AMX 500 operating at 500.13 MHz for ^{1}H and at 470.54 MHz for ^{19}F. The ^{1}H and ^{19}F chemical shifts were measured using the solvent peaks as internal references and then converted into the usual scales corresponding to TMS and $CFCl_3$. The NMR line shapes were simulated using a home-made computer programme described previously for the related ^{15}N,^{15}N′-bis(*p*-fluorophenyl)formamidine (DFFA) [9c,21].

3. Theoretical section

According to Eigen [22], proton transfer between an acid and a base consists of the formation of the reactive complex and the proton transfer within the complex, i.e.

$$\mathrm{A{-}H} + \mathrm{B} \overset{K}{\leftrightarrows} \mathrm{A{-}H\cdots B} \overset{k_{AB}}{\leftrightarrows} \mathrm{A\cdots H{-}B} \leftrightarrows \mathrm{A} + \mathrm{H{-}B}. \tag{1}$$

In Eq. (1) electrical charges are omitted. K represents the equilibrium constant of the complex formation and k_{AB} the intrinsic rate constant. In this study, we deal with a related reaction where a base catalyzes the intramolecular proton transfer between two degenerate forms of the donor, i.e.

$$\mathrm{A'{-}H} + \mathrm{B} \overset{K}{\leftrightarrows} \mathrm{A'{-}H\cdots B} \overbrace{\leftrightarrows [\mathrm{A'\cdots H{-}B}] \leftrightarrows [{}'\mathrm{A\cdots H{-}B}] \leftrightarrows}^{k_{AB}} {}'\mathrm{A{-}H\cdots B} \leftrightarrows {}'\mathrm{A{-}H} + \mathrm{B}. \tag{2}$$

Their interconversion may also be referred to as "proton tautomerism". If the base contains also a mobile proton, a base-catalyzed double proton transfer is competing with Eq. (2)

$$\mathrm{AH} + \mathrm{BH^*} \overset{K}{\leftrightarrows} \mathrm{A{-}H\cdots BH^*} \overset{k_{AB}}{\leftrightarrows} \mathrm{AH^*\cdots B{-}H} \leftrightarrows \mathrm{AH^*} + \mathrm{HB}. \tag{3}$$

Usually, for aqueous solutions, or for hydrogen abstractions from carbon, the concentration of the reactive complex A–H···B is very small and the pre-equilibrium does not need be treated explicitly. However, in organic solvents and also in enzymes the situation may be different. If the concentration of the reactive complex is substantial, it can lead to important changes of the reaction orders which have to be recognized for a proper interpretation of kinetic data obtained.

The formal kinetic treatment of the above reaction schemes is the same. Therefore, they have to be distinguished either by specific spectroscopic features or by the measurement of kinetic hydrogen/deuterium isotope effects. In the following, we present such a kinetic treatment, with particular emphasis to dynamic NMR. Firstly, we deal with the presence of a single reaction mechanism, and then with a superposition of several reaction mechanisms.

3.1. Formal kinetics of catalyzed proton transfer

In the above reaction schemes k_{AB} represents the rate constant of the central forward single or multiple proton transfer step within the reactive complex. This step is assumed to be rate limiting, and the pre-equilibrium assumed to be very fast. K represents the pre-equilibrium constant of the formation of the reactive complex AB ≡ AHB from the reactants,

$$K = \frac{c_{AB}}{c_A c_B}, \tag{4}$$

where c_A and c_B represent the concentrations of the reactants AH and B, and c_{AB} the concentration of the reactive complex AHB.

As we assume that proton transfer represents the rate limiting step, the reaction rate of the proton donor between two exchange processes catalyzed by B is given by

$$\upsilon = -\frac{dC_A}{dt} = -\frac{dC_B}{dt} = -\frac{dc_{AB}}{dt} = k_{AB} c_{AB}, \tag{5}$$

where $C_A = c_A + c_{AB}$ and $C_B = c_B + c_{AB}$ represent the total concentrations of A and of B. k_{AB} is the intrinsic rate constant in the reactive complex. By NMR one measures the average inverse life times of A or of B between two exchange events given by [21]

$$\tau_A^{-1} = -\frac{1}{C_A}\frac{dC_A}{dt}, \quad \tau_B^{-1} = -\frac{1}{C_B}\frac{dC_B}{dt}, \quad \frac{\tau_B^{-1}}{\tau_A^{-1}} = \frac{C_A}{C_B}, \tag{6}$$

which are the same as the pseudo-first-order rate constants of A and of B. One can then easily show that [9a,21]

$$c_{AB} = \frac{1}{2}\left[-\sqrt{(C_A - C_B)^2 + K^{-2} + 2K^{-1}(C_A + C_B)} + C_A + C_B + K^{-1}\right] \tag{7}$$

and it follows that

$$\tau_A^{-1} = -\frac{\upsilon}{C_A} = \frac{\tau_B^{-1} C_B}{C_A} = \frac{k_{AB}}{2C_A}\left[-\sqrt{(C_A - C_B)^2 + K^{-2} + 2K^{-1}(C_A + C_B)} + C_A + C_B + K^{-1}\right]. \tag{8}$$

Eq. (8) predicts changes of the apparent reaction order as a function of C_A and C_B as illustrated in Fig. 1. Important limiting cases are also assembled in Table 1.

Firstly, we consider the case where K is large. Then, at low concentrations of B, it is totally complexed by

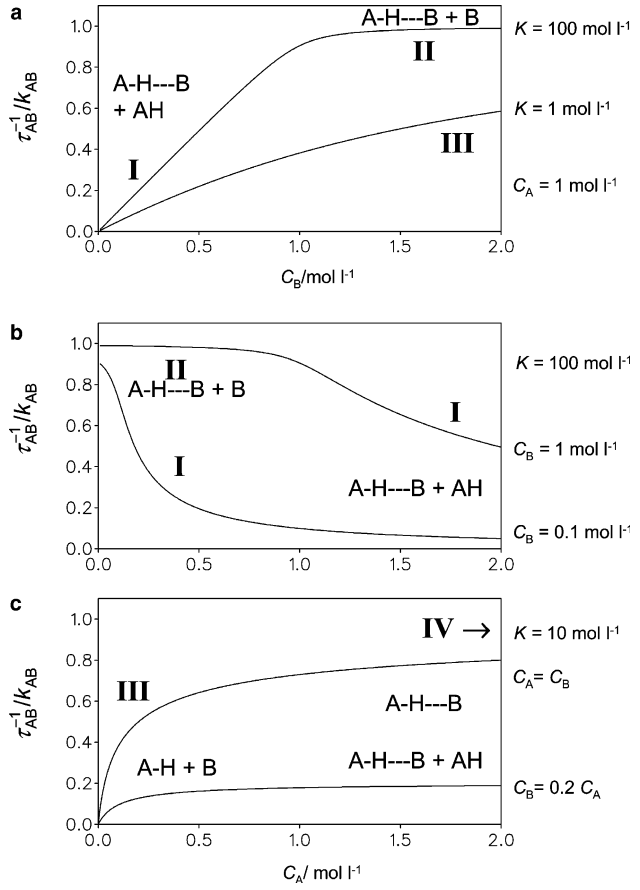

Fig. 1. Inverse life times $\tau_A^{-1} = \tau_{AB}^{-1}$ according to Eq. (8) of a proton donor A – between two proton exchange events catalyzed by a base B – as a function of the total concentrations C_A and C_B and of the equilibrium constant K of the formation of the reactive complex AB. For further explanation see text.

Table 1
The limiting cases of Eq. (8)

Case		K	c_{AB}	$\tau_A^{-1} = \tau_{AB}^{-1}$
I	$C_A > C_B$	Large	C_B	$k_{AB}\frac{C_B}{C_A}$
II	$C_A < C_B$	Large	C_A	k_{AB}
III	$C_A > C_B, C_A < C_B$	Small	KC_B	$k_{AB}KC_B$
IV	$C_B = rC_A$large	Large	r	rk_{AB}

A, whereas the latter is only partially complexed. Therefore, τ_A^{-1} increases linearly with C_B if C_A is kept constant as long as $C_B < C_A$ (case **I**, upper curve in Fig. 1(a)) or decreases when C_A is increased and C_B kept constant (case **I**, Fig. 1(b)). On the other hand, when $C_B > C_A$ (case **II**), A is entirely complexed, and τ_A^{-1} is constant as indicated in Figs. 1(a) and (b).

By contrast, when K is small, and the total concentrations not too large, $c_A \cong C_A$, $c_B \cong C_B$ and c_{AB} is negligible. If follows then that $\tau_A^{-1} = k_{AB}KC_B$ for small concentrations (case **III**) as is illustrated in the lower curve of Fig. 1(a).

Finally, we consider in Fig. 1(c) the case where the ratio $r = C_B/C_A$ is constant. At low concentrations, $\tau_A^{-1} = rk_{AB}KC_B$, but at high concentrations and large values of K Eq. (8) predicts that $\tau_A^{-1} = rk_{AB}$. In both cases, only if r is known from an independent measurement, k_{AB} can be obtained at high concentrations. r is, for example, unity in the case where both A and B are part of a large molecule. In the case where B represents a conformational isomer of A, r corresponds to the equilibrium constant of the conformational isomerism. In the context of this study, r represents the amount of a structural isomer of the proton donor, formed very slowly in the presence of catalytic impurities in an irreversible way. During the time of a typical experiment, r is constant. Then, at least the energy of activation of the process is measurable, as r is independent of temperature, by contrast to a conformational isomerism.

In certain cases the accessible concentration range may be limited, but temperature may be changed more easily. In this case, Eq. (8) may be used in connection with a van't Hoff law for the equilibrium constant of the formation of the reactive complex, and – in the absence of tunneling, by a simple Arrhenius law,

$$K = \exp(-\Delta H/RT + \Delta S/R), \tag{9}$$

$$k_{AB} = A\exp(-E_a/RT), \tag{10}$$

where the symbols have the usual meanings. As we will show later, the combination of Eqs. (8)–(10) can lead to convex Arrhenius curves.

3.2. Superimposed proton transfer mechanisms

We consider now the more general case of a superposition of different reaction mechanisms in which the proton donor A may be involved. Let us assume the presence of different species B or X which catalyze the proton exchange of the donor A. Let us also include the possibility that another donor molecule takes the role of the base. The total inverse life times or the donor are then given by

$$\tau_A^{-1} = \tau_{AA}^{-1} + \tau_{AB}^{-1} + \tau_{AX}^{-1} = k_{AA}c_{AA} + k_{AB}c_{AB} + k_{AX}c_{AX}. \tag{11}$$

Depending on the type of sample prepared and the type of NMR experiment performed, either τ_A^{-1} or the individual components τ_{AA}^{-1}, τ_{AB}^{-1}, τ_{AX}^{-1} or given combinations of the latter are measured as a function of the concentration, from which the true rate constants of the reactive complexes k_{AA}, k_{AB}, k_{AX} may be obtained. To determine which quantity is measured, is part of the kinetic assignment process. If the method employed measures τ_A^{-1}, this quantity is used in an early stage of the analysis, but later replaced by the individual components giving rise to this term.

A special situation arises if the base B can catalyze the tautomerism of A both according to an intramolecular single *and* an intermolecular double proton transfer

pathway depicted in Eqs. (2) and (3). The total inverse life times of A and of B are then given by the sum

$$\tau_A^{-1} = (\tau_{AB}^{-1})^{H} + (\tau_{AB}^{-1})^{HH}, \quad (12)$$

where the first term refers to the single and the second to the double proton transfer case. In favorable cases, both components may be measured individually by NMR as the intramolecular process does not remove scalar coupling of the mobile proton with other nuclear spins in A such as ^{15}N, in contrast to the intermolecular process.

The nomenclature of Eq. (12) is also suitable to include kinetic isotope effects, e.g. the pseudo-first-order rate constants of the isotopic processes can be written as

$$(\tau_{AB}^{-1})^{L} = (\tau_{BA}^{-1})^{L} C_B/C_A \quad \text{with } L = H, D \quad \text{and}$$
$$(\tau_{AB}^{-1})^{LL} = (\tau_{BA}^{-1})^{LL} C_B/C_A \quad \text{with } LL = HH, HD, DD \quad (13)$$

In a similar way, k_{AB}^{L} and k_{AB}^{LL} represent the corresponding intrinsic rate constants in the reactive complexes. For example, k_{AB}^{HD} represents the rate constant of the process where in the reactive complex H of the proton donor A is replaced by D of the base B.

4. Results

In this section, we describe the results of our dynamic NMR measurements performed on **1** in the absence and the presence of added bases which catalyze the tautomerism of this compound. Pseudo-first-order rate constants are assembled in Tables 2–6, whereas Table 7 contains activation parameters resulting from the data.

4.1. Proton exchange and cis/s-trans isomerism of 1,3-bis(4-fluorophenyl)[1,3-$^{15}N_2$]triazene (*1*) in tetrahydrofuran-d_8 in the absence of an added base

4.1.1. NMR spectroscopy

As mentioned in Section 1, in the first stage of this study we looked for a proton self exchange of **1** according to Scheme 2a. As a solvent, THF-d_8 was used which stabilizes the monomer by hydrogen bonding.

In Fig. 2, some typical NMR spectra of two highly purified sealed samples of **1** dissolved at concentrations of 0.5 mol l^{-1} in THF-d_8, with deuterium fractions of $x_D = 0$ and 0.98 in the mobile proton site are depicted. At $x_D = 0$ at 298 K, the ^1H signal of the latter consists of a doublet around 11.4 ppm (Fig. 2(a)), arising from scalar coupling with ^{15}N, where $^1J_{NH} = -93.5$ Hz. The signal position is almost independent of concentration. The signal exhibits some exchange broadening arising from an intermolecular proton exchange process. The latter eventually leads to a coalescence of the doublet signal components.

The ^{19}F spectra in Figs. 2(b) and (c) exhibit two signals around −109 and −117 ppm, indicating the presence of two chemically inequivalent fluorine atoms. No attempts were made to assign the two lines to the two

Table 2
Pseudo-first-order rate constants k_A τ_A^{-1}/s^{-1} of proton exchange of **1** dissolved in THF-d_8

#	Method	T/K	C_A	x_D	k_A	Kin. ass.	#	Method	T/K	C_A	x_D	k_A	Kin. ass.
1	^{19}F-MT	298	0.1	0	75	$(\tau_{AX}^{-1})^{HH}$	11	^{19}F-MT	298	0.7	0	150	$(\tau_{AX}^{-1})^{HH}$
2	^{19}F-MT	298	0.1	0	85	$(\tau_{AX}^{-1})^{HH}$	12	^{1}H-LS	298	0.1	0.98	52	$(\tau_{AX}^{-1})^{HD}$
2a	^{19}F-MT	298	0.1	0	240	$(\tau_{AX}^{-1})^{HH}$	13	^{1}H-LS	298	0.15	0.98	54	$(\tau_{AX}^{-1})^{HD}$
3	^{19}F-MT	298	0.05	0	70	$(\tau_{AX}^{-1})^{HH}$	14	^{1}H-LS	298	0.2	0.98	50	$(\tau_{AX}^{-1})^{HD}$
4	^{19}F-MT	298	0.15	0	155	$(\tau_{AX}^{-1})^{HH}$	15	^{1}H-LS	298	0.3	0.98	80	$(\tau_{AX}^{-1})^{HD}$
5	^{19}F-MT	298	0.2	0	70	$(\tau_{AX}^{-1})^{HH}$	16	^{1}H-LS	298	0.4	0.98	93	$(\tau_{AX}^{-1})^{HD}$
6	^{19}F-MT	298	0.2	0	145	$(\tau_{AX}^{-1})^{HH}$	17	^{1}H-LS	298	0.5	0.98	107	k_{AX}^{HD}
7	^{19}F-MT	298	0.25	0	80	$(\tau_{AX}^{-1})^{HH}$	12	^{19}F-MT	298	0.1	0.98	34	$(\tau_{AX}^{-1})^{DD}$
8	^{19}F-MT	298	0.3	0	170	$(\tau_{AX}^{-1})^{HH}$	13	^{19}F-MT	298	0.15	0.98	31	$(\tau_{AX}^{-1})^{DD}$
9	^{19}F-MT	298	0.5	0	240	$(\tau_{AX}^{-1})^{HH}$	14	^{19}F-MT	298	0.2	0.98	29	$(\tau_{AX}^{-1})^{DD}$
9a	^{19}F-LS	320	0.5	0	1040	$(\tau_{AX}^{-1})^{HH}$	15	^{19}F-MT	298	0.3	0.98	34	$(\tau_{AX}^{-1})^{DD}$
9a	^{19}F-LS	298	0.5	0	630	$(\tau_{AX}^{-1})^{HH}$	16	^{19}F-MT	298	0.4	0.98	60	$(\tau_{AX}^{-1})^{DD}$
9a	^{19}F-MT	275	0.5	0	360	$(\tau_{AX}^{-1})^{HH}$	17	^{19}F-MT	298	0.5	0.98	68	$(\tau_{AX}^{-1})^{DD}$
9a	^{19}F-MT	228	0.5	0	90	$(\tau_{AX}^{-1})^{HH}$	18	^{19}F-LS	329	0.5	0	880	$(\tau_{AX}^{-1})^{HH} + (\tau_{AW}^{-1})^{HH}$
10	^{19}F-LS	330	0.5	0	440	$(\tau_{AX}^{-1})^{HH}$	18	^{19}F-LS	319	0.5	0	810	$(\tau_{AX}^{-1})^{HH} + (\tau_{AW}^{-1})^{HH}$
10	^{19}F-MT	315	0.5	0	320	$(\tau_{AX}^{-1})^{HH}$	18	^{19}F-LS	314	0.5	0	730	$(\tau_{AX}^{-1})^{HH} + (\tau_{AW}^{-1})^{HH}$
10	^{19}F-MT	298	0.5	0	230	$(\tau_{AX}^{-1})^{HH}$	18	^{19}F-LS	309	0.5	0	870	$(\tau_{AX}^{-1})^{HH} + (\tau_{AW}^{-1})^{HH}$
10	^{19}F-MT	280	0.5	0	145	$(\tau_{AX}^{-1})^{HH}$	18	^{19}F-LS	298	0.5	0	640	$(\tau_{AX}^{-1})^{HH} + (\tau_{AW}^{-1})^{HH}$
10	^{19}F-MT	260	0.5	0	85	$(\tau_{AX}^{-1})^{HH}$	18	^{19}F-LS	287	0.5	0	555	$(\tau_{AX}^{-1})^{HH} + (\tau_{AW}^{-1})^{HH}$
10	^{19}F-MT	250	0.5	0	65	$(\tau_{AX}^{-1})^{HH}$	18	^{19}F-LS	278	0.5	0	370	$(\tau_{AX}^{-1})^{HH} + (\tau_{AW}^{-1})^{HH}$
10	^{19}F-MT	240	0.5	0	55	$(\tau_{AX}^{-1})^{HH}$	18	^{19}F-LS	258	0.5	0	185	$(\tau_{AX}^{-1})^{HH} + (\tau_{AW}^{-1})^{HH}$
10	^{19}F-MT	230	0.5	0	35	$(\tau_{AX}^{-1})^{HH}$	18	^{19}F-LS	238	0.5	0	70	$(\tau_{AX}^{-1})^{HH} + (\tau_{AW}^{-1})^{HH}$

#, sample number; MT, magnetization transfer experiments; LS, line shape analysis; τ_{AX}^{-1}, inverse life times of fluorine atoms of A = **1** between two intermolecular exchange processes catalyzed by the structural isomer X = **4** (Scheme 2); Kin. ass., kinetic assignment of τ_{AX}^{-1} to specific processes LL = HH, HD, DD. C_A in mol l^{-1}. $(\tau_{AW}^{-1})^{HH}$ inverse life time of fluorine atoms of A = **1** part arising from exchange with added water in sample #18 where $C_{H2O} = 0.5$ mol l^{-1}.

Table 3
Static and dynamic NMR parameters of solutions of 1,3-bis(4-fluorophenyl)[1,3-$^{15}N_2$]triazene (**1** ≡ **A**) with dimethylamine (**2** ≡ **B**) in methylethyl-ether-d_8

T/K	^{1}H				^{19}F				
	δ	W_0	$(\tau_{AB}^{-1})^{H}$	$(\tau_{AB}^{-1})^{HH}$	δ/ppm	$\Delta\nu$	W_0	$(\tau_{AB}^{-1})^{H} + (\tau_{AB}^{-1})^{HH}$	$(\tau_{AB}^{-1})^{H}$
$C_A = 0.1$ mol l^{-1}, $C_B = 0.028$ mol l^{-1}, $x_D = 0$									
298	10.80	5	–	400	−113.43	2770	5	2500	2100
198	11.47	6	–	280	−112.82	2874	6	1850	1570
168	11.72	6	900	160	−112.46	2916	6	1050	890
158	11.77	6	580	105	−112.38	2924	6	700	600
148	11.81	6	290	≈70	−112.33	2928	6	350	280
138	11.84	8	160	≈40	−112.23	2934	8	190	150
	δ	W_0	$(\tau_{AB}^{-1})^{H}$	$(\tau_{AB}^{-1})^{HD}$	δ	$\Delta\nu$	W_0	$(\tau_{AB}^{-1})^{D} + (\tau_{AB}^{-1})^{DD}$	$(\tau_{AB}^{-1})^{Da}$
$C_A = 0.1$ mol l^{-1}, $C_B = 0.041$ mol l^{-1}, $x_D = 0.98$									
298	10.78	5	–	450	−113.38	2770	5	3200	2900
198	11.56	6	–	245	−112.80	2880	6	2650	2490
178	11.70	6	–	160	−112.67	2950	6	1750	1640
168	11.76	6	1500	135	−112.54	2928	6	1250	1160
158	11.82	6	900	90	−112.43	2934	6	800	740
148	11.87	6	520	≈65	−112.34	2930	6	460	420
138	11.91	8	240	≈50	−112.23	2936	8	230	200

T, temperature; δ, chemical shift in ppm of the NH signal of **1** or average chemical shift of the two fluorine nuclei of **1**; ^{1}H, analysis of the ^{15}N–^{1}H signal of **1**; ^{19}F, analysis of the fluorine signals of **1**; $\Delta\nu$, chemical shift difference of the two fluorine signals in Hz at 470.54 MHz; W_0, residual line width in Hz; C_A, total concentration of **1**; C_B, total concentration of **2**; x_D, deuterium fraction in the mobile proton sites; $(\tau_{AB}^{-1})^{L}$, L = H, D, contribution in s^{-1} of the intramolecular catalyzed proton transfer to the total exchange rate; $(\tau_{AB}^{-1})^{LL}$, LL = HH, HD, DD, contributions in s^{-1} of the intermolecular catalyzed proton transfer. For further explanation see Table 2 and text.

[a] Extrapolated assuming Eq. (16), and in particular the rule of the geometric mean, $(\tau_{AB}^{-1})^{DD} \cong (\tau_{AB}^{-1})^{HD}/1.5$.

fluorine positions of **1**. At 238 K, the signals of the deuterated species are very sharp, whereas the signals of the non-deuterated samples are somewhat broadened by a slow exchange. The expanded spectra of Figs. 2(d) and (e) indicate two additional very weak lines at −110.3 and −111.8 ppm with equal intensities. We assign these signals to a s-*cis* form of **1** as illustrated in Fig. 2. By integration with the ^{13}C satellite signals we estimate a *cis–trans* ratio of about 1:300. We note that an s-*cis*/s-*trans* isomerization has not been observed before for diaryltriazenes by NMR spectroscopy, in contrast to other techniques such as flash photolysis [23]. At 298 K the s-*cis*/s-*trans* isomerism is fast, and coalesced signals are obtained. At $x_D = 0.98$, the high-field signal is broader than the low-field signal, arising from residual exchange broadening: the isomerism is not fast enough and the chemical shift difference between s-*cis* and s-*trans* forms are larger for the nuclei resonating at high field. The differential line width does not appear at $x_D = 0$ because the line widths are here larger, arising from intermolecular proton transfer. This process is slower in the deuterated sample because of a kinetic isotope effect.

In order to obtain values of the pseudo-first-order proton exchange rates τ_A^{-1} of **1**, we performed ^{19}F magnetization transfer experiments in the rotating frame [24]. Both the total concentration C_A of **1** and the deuterium fraction x_D in the mobile proton site were varied.

An example of these measurements is depicted in Fig. 3. The decay of the signals in the "parallel" experiment (Fig. 3(a)) is governed by the longitudinal relaxation time in the rotating frame, $T_{1\rho}$ which was of the order of seconds. In the "antiparallel" experiment (Fig. 3(b)) an exponential decay of the absolute sum of the two signal intensities is observed, governed by the chemical exchange according to [24]

$$I(t) = I(0)\exp[-(2\tau_A^{-1} + 1/T_{1\rho})t]. \quad (14)$$

By non-linear least squares fit a value of $\tau_A^{-1} = 68$ s^{-1} was determined for this sample as indicated in Fig. 3(c).

4.1.2. Kinetic analysis

The kinetic data obtained for DFTA in the absence of an added base are assembled in Table 2. We measured the inverse proton lifetimes τ_A^{-1} as a function of the total concentration C_A of **1** at $x_D = 0$ and 0.98 as depicted in Fig. 4. Unfortunately, in the absence of an added base, we could not obtain reproducible values as is illustrated in Fig. 4(a). When we optimized the sample preparation, the values of τ_A^{-1} were substantially reduced. Within a given series of samples, the values were located on one of the curved solid lines, exhibiting little dependence on concentration.

These observations are not in agreement with the proton self-exchange mechanism according to Scheme 2a, where the partner is a second molecule of **1**. As the observed exchange leads to a loss of the ^{15}NH-coupling, this exchange process must arise from a replacement of the mobile proton of **1** by a mobile proton of an impurity X present in the samples in different amounts

Table 4
Static and dynamic NMR parameters of solutions of 1,3-bis(4-fluorophenyl)[1,3-$^{15}N_2$]triazene (**1** ≡ **A**) with trimethylamine (**3** ≡ **B**) in methylethylether-d_8

T/K	^{1}H				^{19}F			
	δ	W_0	$(\tau_{AB}^{-1})^H$	$(\tau_{AX}^{-1})^{HH}$	δ	$\Delta\nu$	W_0	$(\tau_{AB}^{-1})^H$
$C_A = 0.1$ mol l^{-1}, $C_B = 0.02$ mol l^{-1}, $x_D = 0$								
298	10.96	5	>1400	200	−110.90	2790	5	3300
279	11.10	5	>1400	140	−110.76	2810	5	2750
259	11.24	5	>1400	80	−110.65	2830	5	2100
249	11.30	5	>1400	60	−110.62	2840	5	1800
239	11.37	5	>1500	40	−110.57	2850	5	1500
229	11.43	5	1200	30	−110.50	2860	5	1300
219	11.50	5	970	20	−110.42	2870	5	1000
208	11.57	5	740	–	−110.37	2880	5	800
198	11.64	5	570	–	−110.30	2890	5	600
188	11.72	5	440	–	−110.24	2895	5	450
178	11.80	5	320	–	−110.16	2899	5	320
167	11.88	5	220	–	−110.08	2903	5	210
157	11.97	6	130	–	−109.99	2907	6	–
147	12.07	6	80	–	−109.90	2911	6	–
137	12.17	8	40	–	−109.80	2914	8	–
	δ	W_0	$(\tau_{AB}^{-1})^H$	$(\tau_{AX}^{-1})^{HD}$	δ	$\Delta\nu$	W_0	(τ_{AB}^{-1})D
$C_A = 0.1$ mol l^{-1}, $C_B = 0.02$ mol l^{-1}, $x_D = 0.98$								
298	10.96	5	>1500	150	−110.96	2770	5	3200
279	11.10	5	>1500	90	−110.78	2810	5	2600
259	11.24	5	>1500	50	−110.66	2830	5	2050
249	11.30	5	>1500	40	−110.61	2840	5	1800
239	11.37	5	>1500	30	−110.55	2850	5	1500
229	11.43	5	1200	–	−110.49	2860	5	1250
219	11.50	5	970	–	−110.43	2870	5	1000
208	11.58	5	740	–	−110.39	2880	5	800
198	11.64	5	570	–	−110.32	2890	5	620
188	11.72	5	420	–	−110.25	2895	5	450
178	11.80	5	300	–	−110.15	2899	5	320
167	11.89	5	205	–	−110.10	2903	5	210
157	11.96	6	130	–	−110.01	2907	6	130
147	12.07	6	70	–	−109.91	2911	6	–
137	12.18	8	40	–	−109.82	2914	8	–

For explanation of symbols see Tables 2, 3 and text.

depending on the sample history. The rate constants measured can then be specified as

$$\tau_A^{-1} = (\tau_{AX}^{-1})^{HH} \tag{15}$$

as indicated in Table 2. A priori, X could be either (i) a solvent impurity or an impurity introduced by another way into the sample, for example from the inner glass surface of the NMR tube, or (ii) a species whose concentration is directly related to the presence of **1**, for example compound **4** (Scheme 2). For (i) we expect that $C_X \approx$ constant in a given series of samples prepared from the same substance and solvent lots, whereas for (ii) the concentration of the impurity should be proportional to the concentration of **1**, i.e. $C_X = rC_A$. Case (i) was addressed in the previous section and leads to graphs of the type which were depicted in Fig. 1(b), i.e. to a decrease of the pseudo-first-order rate constants τ_A^{-1} with increasing concentration C_A. By contrast, graphs of the kind depicted in Fig. 1(c) are expected for case (ii). The results of Fig. 4(a) indicate that case (ii) is realized here. This means that within a given sample series, at low concentrations a second-order rate low is observed where τ_A^{-1} increases linearly with C_A, and at high concentrations a first-order rate law is observed where $\tau_A^{-1} = rk_{AX}$ remains constant. This is because at high concentrations X is totally hydrogen bonded to the proton donor **1**. If r were the same in all series of samples, only a single curve should be observed for a given temperature. This case would be realized if, for example, a second molecule of **1**, possibly also in the *cis*-form, would catalyze the exchange. However, this is apparently not the case. Therefore, we assign r the residual exchange of **1** to catalysis by the structural isomer **4**, which is generated by acidic impurities, even hydrophilic glass surfaces. Unfortunately, as the ratio $r = C_X/C_A$ is unknown in a given series of samples, we cannot determine the rate constant k in the reactive complex. Note that the equilibrium constant of the association of X with **1** was set to the value of

Table 5
Pseudo-first-order rate constants of the intra- and the intermolecular proton exchange of 1,3-bis(4-fluorophenyl)[1,3-$^{15}N_2$]triazene (**1**) (**1** ≡ A) in methylethylether-d_8 catalyzed by dimethylamine (**2** ≡ B)

T/K	$(\tau_{AB}^{-1})^{H}$	$(\tau_{BA}^{-1})^{H}$	$(\tau_{AB}^{-1})^{HH}$	$(\tau_{BA}^{-1})^{HH}$	$(\tau_{AB}^{-1})^{D}$	$(\tau_{BA}^{-1})^{D}$	$(\tau_{BA}^{-1})^{H}/(\tau_{BA}^{-1})^{D}$	$(\tau_{AB}^{-1})^{HD}$	$(\tau_{BA}^{-1})^{HD}$	$(\tau_{BA}^{-1})^{HH}/(\tau_{BA}^{-1})^{HD}$
138	150[a]	530[a]	–	–			–	–	–	–
138	160[a]	560[a]	–	–	–	–	–	–	–	–
138	240[b]	590[b]	–	–	200[b]	490[a]	1.20	–	–	–
148	280[a]	980[a]	–	–	–	–	–	–	–	–
148	290[a]	1020[a]	–	–		–	–	–	–	–
148	520[b]	1270[b]	–	–	420[b]	1030[b]	1.24	–	–	–
158	580[a]	2040[a]	105[a]	375[a]			–	–	–	1.7
158	600[a]	2110[a]	–	–	–	–	–	–	–	–
158	900[b]	2200[b]	–	–	740[b]	1810[b]	1.21	90[b]	220	1.7
168	890[a]	3120[a]	160[a]	570[a]	–	–	–	–	–	1.7
168	900[a]	3160[a]	–	–	–	–	–	–	–	
168	1500[b]	3660[b]	–	–	1160[b]	2830[b]	1.29	135[b]	330	1.7
178	–	–	–	–	1640[b]	4000[b]		160[b]	390	–
198	1570[a]	5510[a]	280[a]	1000[a]	–	–	–	–	–	1.7
198	–	–	–	–	2490[b]	6080[b]		245[b]	600	1.7
298	2100[a]	7370[a]	400[a]	1430[a]	–	–		–	–	1.3
298	–	–	–	–	2900[b]	7080[b]		450[b]	1100	1.3

Inverse life time or pseudo-first-order rate constant in s^{-1} of the proton exchange catalyzed by B. Intramolecular exchange: $(\tau_{AB}^{-1})^{L} = (\tau_{BA}^{-1})^{L} C_B/C_A$, L = H, D, intermolecular exchange $(\tau_{AB}^{-1})^{LL} = (\tau_{BA}^{-1})^{LL} C_B/C_A$, LL = HH, HD. $C_A = 0.1$ mol l^{-1} of A in all samples.
[a] $C_B = 0.0028$ mol l^{-1}.
[b] $C_B = 0.0041$ mol l^{-1}.

Table 6
Pseudo-first-order rate constants of the intramolecular proton exchange of 1,3-bis(4-fluorophenyl)[1,3-$^{15}N_2$]triazene (**1**) (**1** ≡ A) in methylethylether-d_8 catalyzed by trimethylamine (**3** ≡ B)

T/K	$(\tau_{AB}^{-1})^{H}$	$(\tau_{BA}^{-1})^{H}$	$(\tau_{AB}^{-1})^{D}$	$(\tau_{BA}^{-1})^{D}$	$(\tau_{BA}^{-1})^{H}/(\tau_{BA}^{-1})^{D}$
157	130	650	130	650	1.00
167	220	1100			–
167	210	1050	–	–	–
167	205	1025	210	1050	0.98
178	320	1600	–		–
178	300	1500	320	1600	0.94
188	440	2200	–	–	
188	450	2250	–	–	
188	420	2100	450	2250	0.93
198	600	3000	–	–	–
198	570	2850	620	3100	0.92
208	800	4000	–	–	
208	740	3700	800	4000	0.93
219	970	4850	1000	5000	0.97
219	1000	5000	–	–	–
219	970	4850	–	–	–
229	1300	6500	–	–	–
229	1200	6000	1250	6250	0.96
239	–	–	1500	7500	–
249	–	–	1800	1800	–
259	–	–	2050	2050	–
279	–	–	2600	2600	–
298	–	–	3200	3200	–

For the explanation of symbols see Table 5. $C_A = 0.1$ mol l^{-1}, $C_B = 0.02$ mol l^{-1} in all cases.

Table 7
Activation parameters of the base catalyzed intra- and intermolecular proton transfer of **1**

	Solvent	ΔH^{L}	ΔS^{L}	E_a^{H}	$\log(A^{H}/s^{-1})$	E_a^{D}	$\log(A^{D}/s^{-1})$	ΔH^{LL}	ΔS^{LL}	E_a^{HH}	$\log(A^{HH}/s^{-1})$	E_a^{HD}	$\log(A^{HD}/s^{-1})$
1 + **2**	MEE	−18	−95	19	11	19.3	11	−18.5	−100	21.1	10.9	21.9	11.5
1 + **3**	MEE	−15.4	−95	23.2	11.5	23.2	11.5	–	–	–	–	–	–
1 + H_2O	THF	–	–	–	–	–	–	–	–	19	–	–	–
1 + **X**	THF	–	–	–	–	–	–	–	–	17	–	18	–

ΔH and E_a in kJ mol^{-1}, ΔS in J K^{-1} mol^{-1}, A in s^{-1}. MEE: methylethylether-d_8, THF: tetrahydrofuran-d_8.

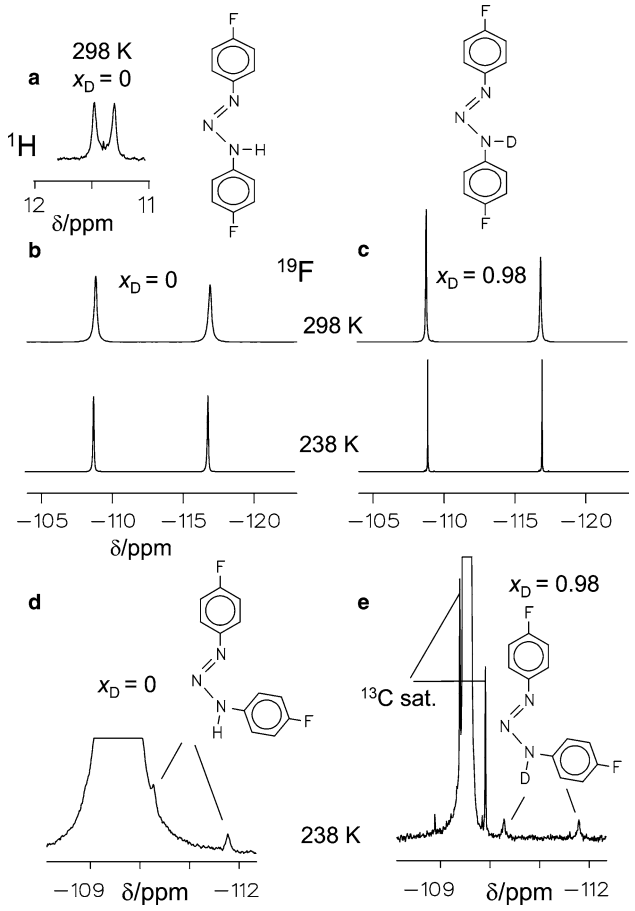

Fig. 2. NMR signals of highly purified samples of **1** dissolved at a concentration of $C_A = 0.5\ \mathrm{mol\,l^{-1}}$ in THF-d_8, at deuterium fractions of $x_D = 0$ and 0.98 in the mobile proton site. (a) ^{1}H signal of the NH proton (500.13 MHz). (b)–(e) Corresponding $\{^1H\}^{19}F$ signals (470.54 MHz). For further explanation see text.

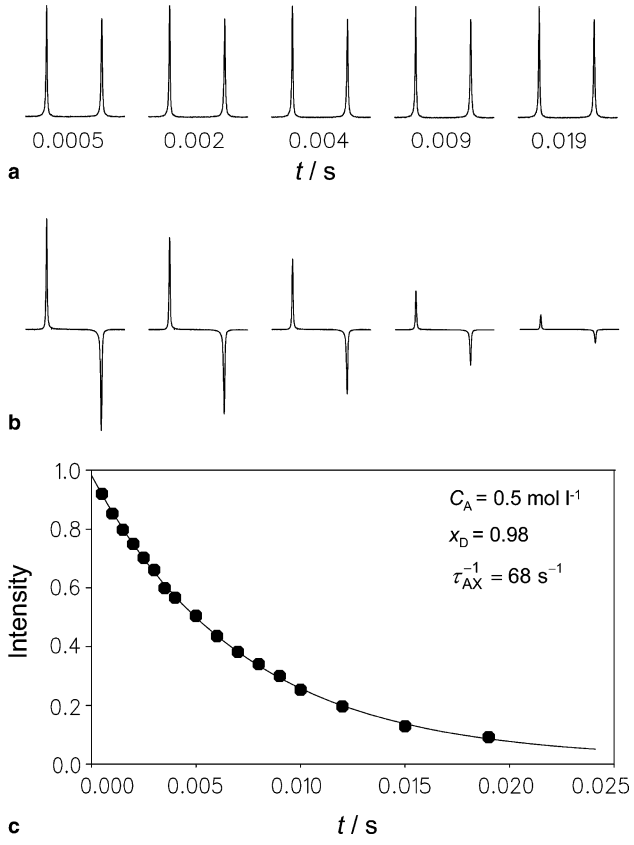

Fig. 3. ^{19}F magnetization transfer experiments in the rotating frame according to [24] performed on **1** dissolved in THF-d_8. Experimental conditions: 299 K , $C_A = 0.5\ \mathrm{mol\,l^{-1}}$, $x_D = 0.98$, ^{19}F Larmor frequency 282.37 MHz, initial $90_x°$ pulse 8.8 μs, spin locking pulse strength 10 kHz in y-direction, length t in s. (a) Parallel experiment with no delay between initial $90_x°$ pulse and spin locking pulse, (b) antiparallel experiment with a delay of $(2\Delta\nu)^{-1} = 299.4$ μs, where $\Delta\nu$ is the chemical shift difference between the two fluorine signals in Hz. (c) Data analysis according to Eq. (14). k_A corresponds to the pseudo-first-order rate constant of the interconversion of the two fluorine nuclei by deuteron transfer. In the later analysis, we assign k_A to k_{AX}, where X represents an unidentified impurity. For further explanations see text.

$K = 21.4\ \mathrm{l\,mol^{-1}}$ for all curves in Fig. 4 which reproduces well the kinetic data.

As r can be regarded as independent of temperature, we measured for two selected samples, both with $C_A = 0.5\ \mathrm{mol\,l^{-1}}$, τ_A^{-1} as a function of temperature. The results are included in Table 2 (samples #9a and #10). We found the same energy of activation of 16.2 kJ mol^{-1} for both samples, although the inverse lifetimes at 298 K were different, i.e. 630 and 230 s^{-1} for sample #9a and #10.

In Fig. 4(b) are symbolized the corresponding values of $\tau_A^{-1} = (\tau_{AX}^{-1})^{DD}$ obtained by ^{19}F NMR at a deuterium fraction of $x_D = 0.98$ by full squares. On average, deuteration lowers the exchange rates due to a kinetic isotope effect. However, as the different samples contain different amounts of **4**, it is not possible to obtain kinetic isotope effects from samples with different deuterium fractions. However, this problem could be partially circumvented by analyzing the line widths of the ^{1}H–^{15}N doublets by ^{1}H NMR (see Fig. 2(a)) for each of the samples with $x_D = 0.98$, from which we obtained the values of $(\tau_{AX}^{-1})^{HD}$ listed in Table 2. Now, for a given sample at $x_D = 0.98$ we obtained the kinetic isotope effects $(\tau_{AX}^{-1})^{HD}/(\tau_{AX}^{-1})^{DD} \cong k_{AX}^{HD}/k_{AX}^{DD}$, which are symbolized by open squares in the upper part of Fig. 4(b). These effects may not be very precise, but they are independent of the concentration of X. Overall, a value of $(\tau_{AX}^{-1})^{HD}/(\tau_{AX}^{-1})^{DD} = 1.6$ is obtained at 298 K.

Therefore, these results support strongly the interpretation that the impurity X corresponds to the decomposition product **4** (see Scheme 1). The latter is protonated by **1**, and either the original or one of the two other amino protons are transferred back to the base. This explains the loss of the ^{15}N–^{1}H splitting by this exchange process. Because of the difficulty in making samples with known concentrations of **4**, we did not pursue this reaction further.

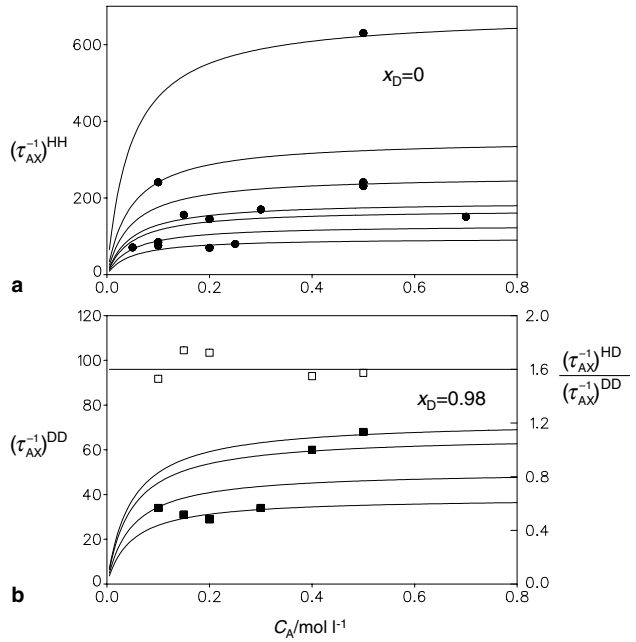

Fig. 4. (a) Experimental and calculated dependence of the proton exchange rates $\tau_{AX}^{-1} = (\tau_{AX}^{-1})^{HH}$ in s^{-1} (see Table 2) of **1** dissolved in THF-d_8 determined by ^{19}F magnetization transfer as a function of the total concentration C_A of **1**. Conditions: 299 K, $x_D = 0$. The calculated curves were generated using Eq. (8) assuming catalysis of the proton exchange of **1** by an unknown impurity X, with $C_X = rC_A$. The solid curves are defined by the same value of $K = 21.41$ mol^{-1} and by varying values of the product rk_{AX}^{HH}, given by the values at high concentrations C_A. (b) As (a) but $x_D = 0.98$. The solid rectangles refer to $\tau_{AX}^{-1} = (\tau_{AX}^{-1})^{DD}$ and the open rectangles to the kinetic isotope effect $(\tau_{AX}^{-1})^{HD}/(\tau_{AX}^{-1})^{DD}$, where $(\tau_{AX}^{-1})^{HD}$ was determined by ^1H and $(\tau_{AX}^{-1})^{DD}$ by ^{19}F line shape analysis. The value of K was the same as in (a).

4.1.3. The effect of added water

In order to elucidate the effect of water on the proton exchange rates of **1** we added 0.5 mol l^{-1} water by vacuum transfer to sample #10 which contained 0.5 mol l^{-1} of **1**, resulting in sample #18, and measured the total pseudo-first-order rate constants $\tau_A^{-1} = (\tau_{AX}^{-1})^{HH} + (\tau_{AW}^{-1})^{HH}$ by fluorine NMR as a function of temperature, included in Table 2. The addition of such a large quantity of water had not a dramatic effect on the tautomerism of **1**. At 298 K, τ_A^{-1} increased only from 230 s^{-1} for sample #10 to a value of 640 s^{-1} for sample 18. The energy of activation of the water catalyzed process is about 19 kJ mol^{-1}, however, a detailed analysis is not possible because of the problem of the formation of hydrogen bonded water clusters and the reduced solubility of water at lower temperatures.

4.2. Proton exchange of 1,3-bis(4-fluorophenyl)[1,3-$^{15}N_2$]triazene (*1*) with dimethylamine and trimethylamine in methylethylether-d_8

In order to better understand the acid–base properties of **1** we checked whether proton exchange is more efficiently catalyzed by stronger bases as compared to water. Therefore, we choose dimethylamine **2** as a simple base containing an exchangeable proton. In order to characterize the effect of the latter, we also performed studies with trimethylamine **3** for comparison. In fact, both bases were found to be very efficient catalysts and the proton exchange rates were much faster as compared to pure **1** and **1** with water. Therefore, we changed the solvent to methylethylether-d_8 instead of THF-d_8 which allowed us to reach lower temperatures down to 138 K.

4.2.1. NMR spectroscopy

In Figs. 5 and 6 are depicted the superposed experimental and calculated ^1H and $^{19}F\{^1H\}$NMR spectra of **1** without and with deuteration of the mobile proton site in the presence of small quantities of dimethylamine **2**. Because of its small concentration, the NH-signal of **2** could not been observed. In a separate sample of **2** in methylethylether-d_8, the chemical shift of the NH-proton was found to be 2.8 ppm in the temperature range between 140 and 200 K. At low temperatures, we observe an ^1H–^{15}N doublet of **1** around 12 ppm as expected, characterized by a coupling constant of $^1J_{NH} = -93.5$ Hz. The line shapes of this signal are independent of the deuterium fraction. The doublet does not exhibit only two sharp outer lines but also additionally a

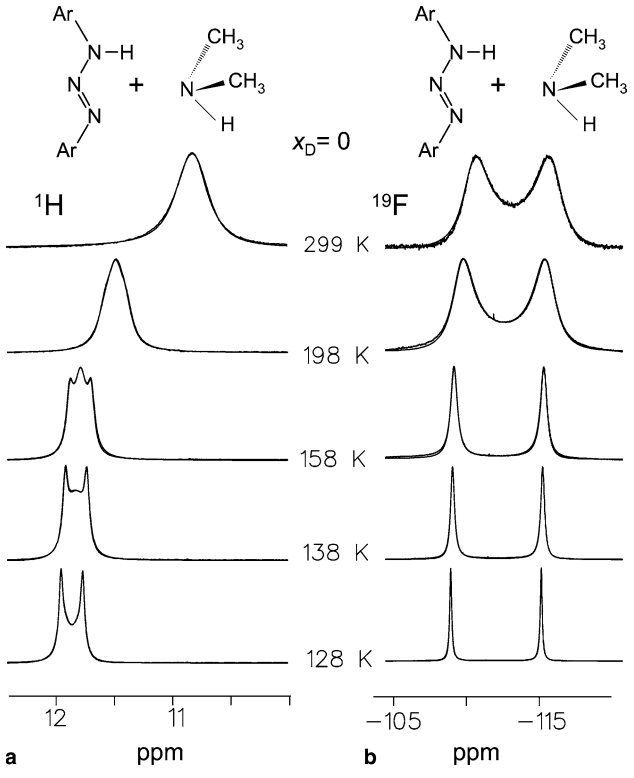

Fig. 5. Superimposed experimental and simulated temperature dependent ^1H signals (500 MHz) (a) and ^{19}F NMR signals (b) of a solution of **1** (0.1 mol l^{-1}) and of dimethylamine **2** (0.0028 mol l^{-1}) in methylethylether-d_8. The deuterium fraction in the mobile proton site of **1** is $x_D = 0$. For further explanation see text.

broad center part which sharpens at higher temperatures into a triplet with $^1J_{NH} = 47$ Hz, arising from a coupling to both ^{15}N atoms of **1**. The observation of the triplet proves the presence of a fast intramolecular proton transfer according to Scheme 2b mediated by **2**. Intermolecular proton exchange alone would lead to a doublet–singlet transition and broaden and eventually coalesce all lines of the signal [21]. This phenomenon takes place at higher temperatures. At room temperature, the signal is broad, arising from proton exchange with the mobile proton of **2**. For the deuterated sample (Fig. 6), the ^1H signals of the residual protonated species exhibits similar features as in Fig. 5. Again the doublet–triplet transition has already occurred before the onset of line broadening arising from intermolecular proton exchange with **2**.

The ^{19}F signals are sharp at low temperatures, and broaden considerably as temperature is raised. They exhibit a very remarkable feature: at 198 K the lines exhibit already a large exchange broadening, but even a temperature increase to 299 K does not lead to a coalescence of the two fluorine lines. This means that the proton exchange does not substantially increase with increasing temperature, a very unusual finding which – as explained in more detail below – arises from the fact that on one hand the rate constants of proton transfer in the acid–base complex increase with increasing temperature, but that on the other hand the reacting complex itself also dissociates into the non-reactive constituents. After deuteration, the exchange rates decrease somewhat; however, as in the deuterated sample the concentration of the base was 0.0041 mol l^{-1} as compared to 0.0028 mol l^{-1} for the non-deuterated sample, this decrease is only revealed by the kinetic analysis.

In order to confirm the intramolecular base-catalyzed proton transfer of **1** we measured the effects of added trimethylamine **3**. In Figs. 7 and 8 are depicted the superimposed experimental and calculated variable temperature ^1H and ^{19}F NMR spectra of **1** and of its deuterated analog (both 0.1 mol l^{-1}) containing 0.02 mol l^{-1} trimethylamine **3**. The ^{19}F NMR spectra are very similar as those in Figs. 5 and 6. Especially the doublet–triplet transition is well pronounced because the base cannot exchange protons with **1**. A small intermolecular proton exchange with the above-mentioned unidentified impurity X gives rise to some line broadening at higher temperatures.

4.2.2. Kinetic analysis

The line shape analysis of the spectra in Figs. 5–8 are straightforward and were done using techniques and computer programs described previously [21]. All

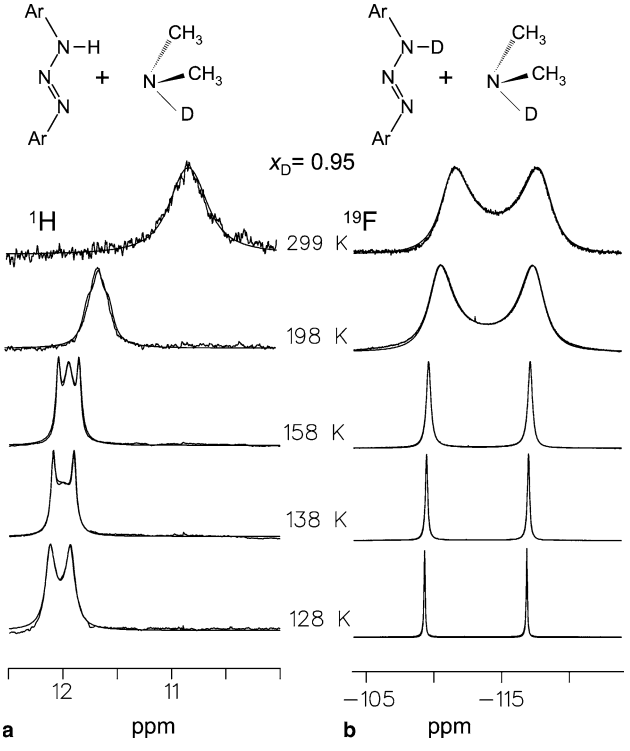

Fig. 6. Superimposed experimental and simulated temperature dependent ^1H signals (500 MHz) (a) and ^{19}F NMR signals (b) of a solution of **1** (0.1 mol l^{-1}) and of dimethylamine **2** (0.0041 mol l^{-1}) in methylethylether-d_8. The deuterium fraction in the mobile proton site of **1** is $x_D = 0.95$. For further explanation see text.

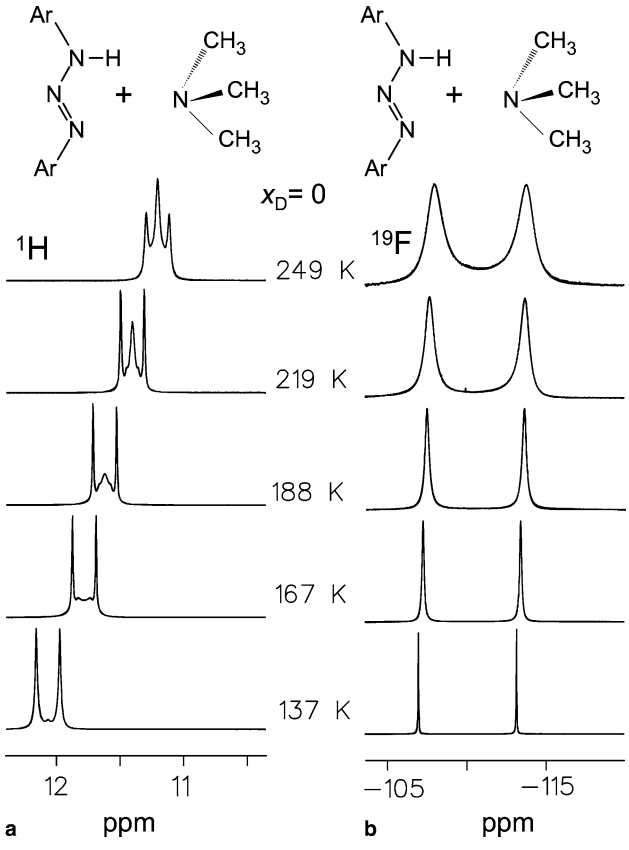

Fig. 7. Superimposed experimental and simulated temperature dependent ^1H signals (500 MHz) (a) and ^{19}F NMR signals (b) of a solution of **1** (0.1 mol l^{-1}) and of trimethylamine **3** (0.02 mol l^{-1}) in methylethylether-d_8. The deuterium fraction in the mobile proton site of **1** is $x_D = 0$. For further explanation see text.

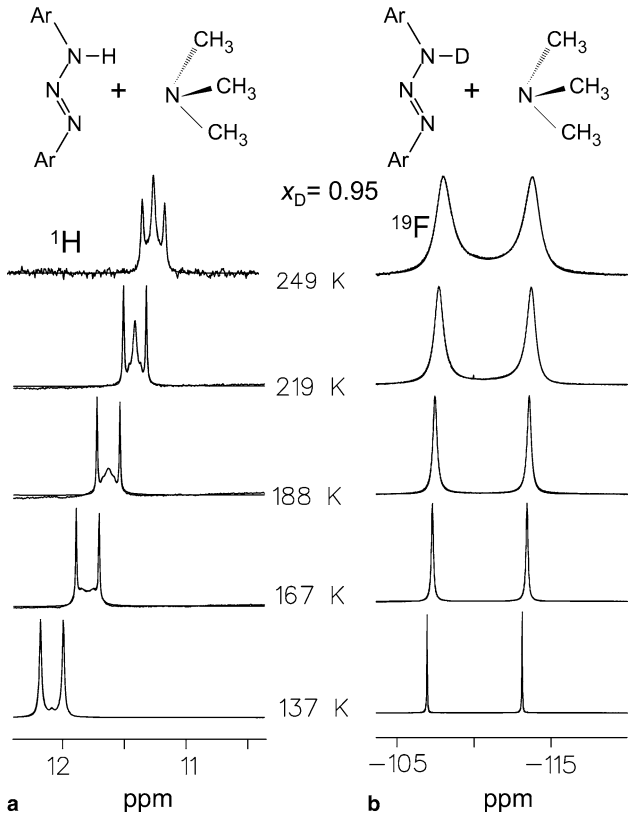

Fig. 8. Superimposed experimental and simulated temperature dependent ^{1}H signals (500 MHz) (a) and ^{19}F NMR signals (b) of a solution of **1** (0.1 mol l^{-1}) and of trimethylamine **3** (0.02 mol l^{-1}) in methylethylether-d_8. The deuterium fraction in the mobile proton site of **1** is $x_D = 0.96$. For further explanation see text.

parameters which describe the spectra are assembled in Tables 3 and 4, and the kinetic results in Tables 5 and 6. For the kinetic analysis we proceeded as follows.

In a first step we simulated the ^{1}H–^{15}N signals of the sample with trimethylamine **3** at $x_D = 0$. The doublet–triplet transition observed is typical for an intramolecular single proton transfer according to Scheme 2b. Therefore, the line shape analysis directly yields the pseudo-first-order rate constants or inverse proton life times $\tau_A^{-1} = (\tau_{AB}^{-1})^H$ of **1** in the presence of **3**. As the outer lines of the ^{1}H–^{15}N signals of the triplet are not affected by this exchange process, the line width W_0 in the absence of exchange could be obtained directly, which was of the order of 5 Hz. By comparison with the solvent lines, we concluded that this value is determined mainly by the inhomogeneity of the magnetic field, as no sample spinning was employed. Therefore, we used for the line shape analysis of the other samples the line widths of the solvent signals as best approach for W_0. In the temperature region around 230 K and higher, we found broadening of all lines of the ^{1}H–^{15}N signals arising from the slow intermolecular proton exchange with $X \equiv \mathbf{4}$, where the total line width $W = W_0 + \pi(\tau_{AX}^{-1})^{HH}$.

In the second stage we simulated the ^{19}F line shapes, from which the sums $\tau_A^{-1} = (\tau_{AB}^{-1})^H + (\tau_{AX}^{-1})^{HH}$ were obtained at $x_D = 0$. However, it turned out that $(\tau_{AB}^{-1})^H \gg (\tau_{AX}^{-1})^{HH}$, i.e. the contribution from the impurity $X \equiv \mathbf{4}$ to the ^{19}F NMR line shapes could be neglected in the whole temperature range.

The simulation of the spectra of the sample with trimethylamine and a deuterium fraction of $x_D = 0.96$ (Fig. 8) was then straightforward. As expected, from the line shape of the residual ^{1}H–^{15}N signal again values $(\tau_{AB}^{-1})^H$ were obtained, and by ^{19}F NMR the corresponding values of $(\tau_{AB}^{-1})^D$, leading to quite precise kinetic H/D isotope effects listed in Table 6. As we worked in the regime $C_A > C_B$, it was more convenient according to Table 1 to discuss the values of $(\tau_{BA}^{-1})^H = (\tau_{AB}^{-1})^H\ C_A/C_B$ rather than those of $(\tau_{AB}^{-1})^H$, because the values of $(\tau_{BA}^{1})^H$ at low temperatures are equal to the first-order rate constants k_{AB}^L in the reaction complex. Furthermore, as C_A was equal to 0.1 mol l^{-1} and constant in all samples of Fig. 5 to 6, the values of $(\tau_{BA}^{-1})^H$ of the different samples can directly be compared with each other. By division of the values of $(\tau_{BA}^{-1})^H$ and of $(\tau_{BA}^{-1})^D$ obtained by ^{1}H and ^{19}F NMR, we obtain the kinetic isotope effects which are slightly smaller than 1 as indicated in Table 6.

For the simulation of the spectra of **1** in the presence of dimethylamine **2** depicted in Figs. 5 and 6 we proceeded in a similar way. By the simulation of the ^{1}H–^{15}N signals, we obtained again values of $(\tau_{AB}^{-1})^H$ of the intramolecular base-catalyzed proton transfer. The line shapes at $x_D = 0$ depend also on the corresponding pseudo-first-order rate constants $(\tau_{AB}^{-1})^{HH}$ of the intermolecular exchange of **1** with the base **2**, and at $x_D = 0.95$ on the corresponding values of $(\tau_{AB}^{-1})^{HD}$. The values of $(\tau_{AB}^{-1})^{HH}$ are much smaller than those of the intramolecular process, but still much larger than those of $(\tau_{AX}^{-1})^{HH}$ of the slow residual intermolecular exchange. Therefore, the latter values did not affect the line shapes. In Table 5 are listed again the values of $(\tau_{AB}^{-1})^L$ and of $(\tau_{AB}^{-1})^{LL}$, and in addition those of $(\tau_{BA}^{-1})^L$ and of $(\tau_{BA}^{-1})^{LL}$ needed for the discussion. Moreover, the kinetic isotope effects $(\tau_{BA}^{-1})^H/(\tau_{BA}^{-1})^D$ obtained and some values of $(\tau_{BA}^{-1})^{HH}/(\tau_{BA}^{-1})^{HD}$ are included. Values of $(\tau_{BA}^{-1})^{HD}/(\tau_{BA}^{-1})^{DD}$ could not be obtained directly, as $(\tau_{AB}^{-1})^{DD}$ did not affect the ^{19}F line shapes in a significant way because of the dominance of the intramolecular H transfer. Therefore, we used the rule of the geometric mean

$$(\tau_{AB}^{-1})^{DD}/(\tau_{AB}^{-1})^{HD} \cong (\tau_{AB}^{-1})^{HD}/(\tau_{AB}^{-1})^{HH} \qquad (16)$$

in order to estimate $(\tau_{AB}^{-1})^{DD}$ and hence $(\tau_{BA}^{-1})^{DD}$. In particular, an average value of $(\tau_{AB}^{-1})^{DD}/(\tau_{AB}^{-1})^{HD} = (\tau_{BA}^{-1})^{DD}/(\tau_{BA}^{-1})^{HD} \cong 1.5$ was employed in the whole temperature range.

5. Discussion

In this section, we will first address the problem of convex Arrhenius curves, and then discuss the results obtained for the base-catalyzed intra- and intermolecular proton tautomerism of the title compound 1,3-bis(4-fluorophenyl)[1,3-$^{15}N_2$]triazene (**1** ≡ A) dissolved in THF-d_8 and in $CD_3OC_2D_5$. Some preliminary quantum-mechanical calculations are presented in order to assist the interpretation of the kinetic data. In a section devoted to the kinetic H/D isotope effects we will discuss the problem of the concerted vs. stepwise double proton transfer. Finally, some general implications for kinetic studies of proton exchange reactions by NMR will be discussed.

5.1. The occurrence of convex Arrhenius curves

In Section 3, we have treated Eigen's and related schemes of proton transfer between a proton donor A and a base B according to Eqs. (1)–(3), in the regime where a substantial amount of the reactive complex AB in which the proton transfer takes place is formed. Eq. (8) provides an expression of the pseudo-first-order rate constants or average inverse life times of A and B, $\tau_A^{-1} = \upsilon/C_A$ and $\tau_B^{-1} = \upsilon/C_B$ between two exchange events as a function of the following parameters: (i) the total concentrations C_A and C_B, (ii) the equilibrium constant K of the formation of the reactive complex AB, and (iii) the first-order rate constant k_{AB} of proton transfer in the reactive complex. υ represents the reaction rate.

Assuming a simple van't Hoff law (Eq. (9)) and a simple Arrhenius law (Eq. (10)) for the temperature dependence of K and of k_{AB} one obtains convex Arrhenius curves of the kind depicted in Fig. 9.

The intrinsic Arrhenius curves referring to the reactive complex are characterized by dashed lines, characterized by the intrinsic energy of activation, E_{AB} and the intrinsic pre-exponential factor A_{AB}. For intramolecular H atom transfers A_{AB} is normally of the order of 10^{12}–10^{13} s^{-1}, whereas for proton transfers exhibiting zwitterionic intermediates or products A_{AB} is somewhat reduced by one or two orders of magnitude because of solvent reorganisation [25]. Therefore, we use a value of $A_{AB} = 10^{11}$ s^{-1} for the intrinsic proton transfer in the reactive complex. The enthalpy ΔH and the entropy ΔS of the formation of the reactive complex are varied in Fig. 9, leading to the solid convex Arrhenius curves. For simplicity we set C_A to 1 mol l^{-1}.

When both ΔH and ΔS are negative, the equilibrium constant $K \gg 1$ at low temperatures. Assuming that B is the minor component, then all molecules of this kind are present in the reactive complex AB. In this case, Eq. (8) predicts that $\tau_B^{-1} = k_{AB}$, and the solid and dashed curves in Fig. 9(a) coincide.

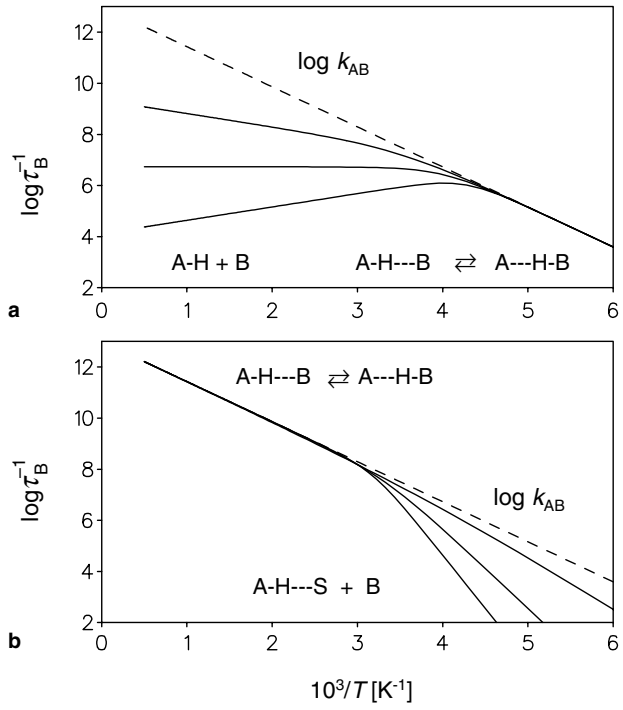

Fig. 9. Inverse life times according to Eqs. (8)–(10) of a proton donor A between two proton exchange events catalyzed by a base B as a function of temperature. Parameters of the Arrhenius curves in the reactive complex: $\log_{10} A = 13$, and $E_a = 7.15$ kcal mol^{-1}. Parameters of the formation of the active complex (a) $\Delta H = -4.78$ kcal mol^{-1}, $\Delta S = 16.73$ cal K^{-1} mol^{-1}, $\Delta H = -7.17$ kcal mol^{-1}, $\Delta S = -28.67$ cal K^{-1} mol^{-1}, $\Delta H = -9.56$ kcal mol^{-1}, $\Delta S = -40.62$ cal K^{-1} mol^{-1}. (b) $\Delta H = 2.39$ kcal mol^{-1}, $\Delta S = 9.56$ cal K^{-1} mol^{-1}, $\Delta H = 7.17$ kcal mol^{-1}, $\Delta S = 23.89$ cal K^{-1} mol^{-1}, $\Delta H = 11.95$ kcal mol^{-1}, $\Delta S = 38.23$ cal K^{-1} mol^{-1}. For further explanation see text.

By contrast, at high temperatures $K \ll 1$, i.e. the reactive complex dissociates. In this case, Eq. (8) predicts that

$$\tau_B^{-1} = kKC_A \exp(-\Delta H/RT)\exp(\Delta S/R)A\exp(-E_a/RT) \quad \text{and} \quad \tau_A^{-1} = kKC_B \tag{17}$$

with the observed activation parameters

$$A_B = C_A A \exp(\Delta S/R) \quad \text{and} \quad E_{aB} = \Delta H + E_{AB}. \tag{18}$$

The observed slope of the Arrhenius curve will be smaller than at low temperatures and may be even negative if $|\Delta H| > E_{AB}$ as illustrated in Fig. 9(a). An abnormally small pre-exponential factor is observed, which is affected by the concentration of A.

On the other hand, one can also conceive a situation where the separated states of A and B are more stable at low temperatures, for example, because of the formation of non-reactive complexes with the solvent S, or a reduced mobility in an enzyme. The reacting state AB may then predominate at high temperatures. This case can be described by positive values of ΔH and ΔS for the formation of the reactive complex from the reactants, leading to the abnormally

large pre-exponential factors and energies of activation at low temperature, as depicted in Fig. 9(b). By contrast, now the Arrhenius curves at high temperatures exhibit a normal pre-exponential factors. However, both situations lead to convex Arrhenius curves.

We note that Kohen et al. [26] have observed a convex Arrhenius curve in the H-transfer reaction of a thermophilic alcohol dehydrogenase (ADH) which might be explained in terms of the situation of Fig. 9(b).

5.2. Arrhenius curves of the base-catalyzed intra- and intermolecular tautomerism of *1*

We are now prepared to discuss the Arrhenius diagrams of the base-catalyzed intra- and intermolecular tautomerism of **1**. In Fig. 10, we have plotted the pseudo-first-order rate constants or average molecular life times of the base-catalyzed proton tautomerism of **1** obtained in this study on a logarithmic scale as a function of the inverse temperature. In Fig. 10(a), we plotted the values of $\tau_B^{-1} = (\tau_{BA}^{-1})^L$, $L = H, D$ which represent the inverse life times of the bases dimethylamine **2** and trimethylamine **3** (see Tables 5 and 6) between two *intramolecular single hydron* exchange events with **1**. As discussed in Fig. 9(a), these values provide at low temperatures the intrinsic rate constants k_{AB}^L. In Fig. 10(b), we plotted the corresponding inverse life times $\tau_B^{-1} = (\tau_{BA}^{-1})^{LL}$ of **2** between two *intermolecular double* hydron transfer events with **1**, which are identical at low temperatures with the rate constants k_{AB}^{LL} of the double proton transfer between **1** and **2**.

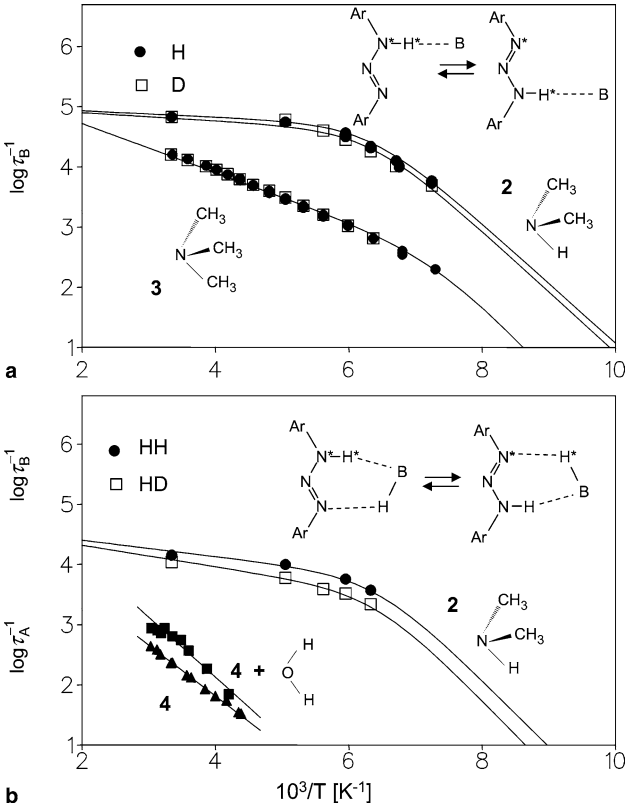

Fig. 10. (a) Arrhenius diagrams of the intramolecular proton and deuteron transfer in 1,3-bis(4-fluorophenyl)[1,3-$^{15}N_2$]triazene (**1**) dissolved at a concentration of 0.1 mol l^{-1} in methylethylether-d_8, catalyzed by the bases dimethylamine (**2**) (0.0028 mol l^{-1} at $x_D = 0$ and 0.0041 mol l^{-1} at $x_D = 0.95$) and trimethylamine **3** (0.02 mol l^{-1} at $x_D = 0$ and $x_D = 0.96$). τ_A^{-1} and τ_B^{-1} represents the average inverse life times of the proton donor A and of the base B between two exchange events. (b) Arrhenius diagrams of the intermolecular proton and deuteron transfer of 1,3-bis(4-fluorophenyl)[1,3-$^{15}N_2$]triazene (**1**) catalyzed by dimethylamine (**2**) (upper curves), catalyzed by water and the decomposition product X (lower curves) assigned to **4** in Scheme 2.

In the case of the reaction with dimethylamine **2** we observe a strong non-linear convex shape of the Arrhenius curve, which could be easily reproduced in terms of Eq. (8) although simple Arrhenius relations (Eq. (10)) for the temperature dependence of k_{AB}^L and of k_{AB}^{LL} as well as van't Hoff relations (Eq. (9)) for the equilibrium constants K of the pre-equilibria in Scheme 2b and c were assumed.

In order to obtain the corresponding activation parameters assembled in Table 7 we proceeded as follows. We first calculated the Arrhenius curve of the intramolecular proton transfer of **1** catalyzed by **2** (upper curves in Fig. 10(a)) by non-linear least squares fit of the data to Eqs. (8)–(10). At low temperatures, where the acid–base complex is fully formed, the energy of activation $E_{AB}^L \approx 19$ kJ mol^{-1} and the pre-exponential factors $A^L \approx 10^{11}$ s^{-1} ($L = H$, D) (Table 7) were obtained.

At high temperatures, the values of $(\tau_{BA}^{-1})^L$ become temperature independent; in this regime the effective slope of the Arrhenius diagram is governed by the difference $E_{AB}^L - \Delta H$ as discussed above. We note that there is a small kinetic H/D isotope effect of about 1.2 (Table 2) on the intramolecular exchange. The Arrhenius curves of the intermolecular exchange (upper curves in Fig. 10(b)) were now simulated assuming that the reaction enthalpies and entropies of the formation of the reactive complexes both processes are similar. It is interesting to note that this intermolecular double proton transfer between **1** and **2** is slower than the "mono"-functional intramolecular transfer (Table 2). We find a small kinetic HH/HD isotope effect of about 1.3 to 1.7 on the intermolecular proton transfer of **1** with **2**.

The nature of the intramolecular base-catalyzed proton transfer was studied in more detail using trimethylamine **3** as a base. Here, the convex curvature of the Arrhenius curve is less pronounced. Assuming that the enthalpy and entropy of the association as well as the pre-exponential factor similar as in the corresponding reaction with **2** , i.e. about 10^{11} s^{-1} (Table 7) we calculated the lower solid line in Fig. 10(a). The activation energy in the reacting complex is 4 kJ mol^{-1} larger as compared to the reaction with **2**. An inverse kinetic

isotope effect of about 0.93–0.97 was obtained (Table 6); as this effect is so close to unity, and the estimated margin of error ± 0.05, we do not discuss this value in detail.

In Fig. 10(b) are included the logarithmic values of $\tau_A^{-1} = \tau_{AX}^{-1}$ obtained for the THF-samples #9a and #10 in the absence of added bases, assigned to the reaction with **4** (Scheme 2). In order to include the data of both samples on the same Arrhenius curve, those of sample #9a were scaled by a factor of 2.7 corresponding to the ratio of inverse lifetimes at 298 K. The graph shows that the energy of activation of 17 kJ mol^{-1} describes well both samples. This factor corresponds then to the ratio of the catalytic base **4** in both samples. The pre-exponential factor could not be obtained as it was not possible to detect **4** directly and to measure its concentration. We estimate values of 0.01 M or smaller. The addition of 0.5 mol^{-1} water to a 0.5 M solution of **1** increases the values of $\tau_A^{-1} = \tau_{AX}^{-1} + \tau_{AW}^{-1}$ only slightly, as indicated in Fig. 10(b). This result indicates that small traces of water are not responsible for the residual tautomerism of **1**.

For each of the samples #12 to #15, containing a deuterium fraction of 0.98 in the mobile proton sites, it was possible to measure the inverse life times $(\tau_{AX}^{-1})^{HD}$ by ^{1}H NMR and the inverse life times $(\tau_{AX}^{-1})^{DD}$ by ^{19}F NMR. Their ratio corresponds to the ratio of the intrinsic rate constants k_{AX}^{HD}/k_{AX}^{DD}, as the concentration of the catalyst X = **4** is the same for both measurements, neglecting isotope effects on the pre-equilibrium. The kinetic isotope effects obtained are of the order of 1.6, consistent with a slightly larger energy of activation of about 18 kJ mol^{-1} for the DD process as compared to the HD process.

The observation of these isotope effects indicates that more than a single proton is exchanged in the residual tautomerism of **1**, most probably a double proton transfer. This finding is consistent with the molecular structure of **4**, where the catalytic active group is the amino group. The reaction must then take place in such a way, that a proton of the amino group of **4** is transferred to **1**, when the mobile proton of **1** is transferred to **4**. There may be, however, a chance of up to 1/3 that the same proton is transferred back to **1**.

Unfortunately, it was not possible to study the reactions of **1** with **4** and with water in more detail, however, the present data show that the basicity of the added bases plays a major role. As **2**, **3** and **4** are expected to be more basic than water, they catalyze the tautomerism of **1** in a more efficient way.

5.3. Quantum-mechanical calculations

In order to corroborate these conclusions and to explore the potential reaction pathways of the intramolecular proton transfer of **1** catalyzed by trimethylamine **3** in a preliminary way we have performed semi-empirical quantum-mechanical calculations with the PM3-MNDO method using the MOPAC package versions 6.0 and 7.0 [27]. We are well aware that the results obtained by this method are only qualitative.

We assumed that the motion of the proton is restricted to a plane spanned by the *x*- and *y*-axes according to Fig. 11, where the plane contains the triazene

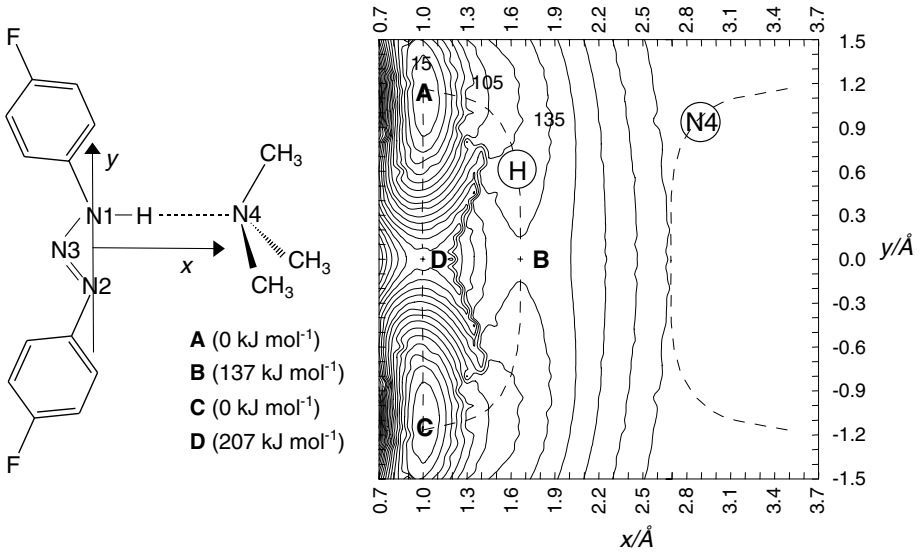

Fig. 11. Potential energy surface of the intramolecular proton transfer in 1,3-bis(4-fluorophenyl)[1,3-$^{15}N_2$]triazene (**1**) catalyzed by trimethylamine (**3**), calculated using the semi-empirical PM3-MNDO method using the MOPAC package version 6.0 [27]. The proton is assumed to move within a plane spanned by the axes *x* and *y*, containing the triazene moiety and the nitrogen atom of the base. The *y*-axis goes through the two terminal nitrogen atoms, the *x*-axis through the center between the terminal nitrogen atoms. All atomic coordinates besides the transferred proton were optimized for each position of the latter. A: initial and C: final state, B: transition state of the base catalyzed and D of the non-catalyzed intramolecular proton transfer. For further explanation see text.

moiety, the two attached carbon atoms, the mobile proton and the nitrogen atom of the base. The *y*-axis goes through the two terminal nitrogen atoms N1 and N3. The origin of the *y*-axis was located midway between these two atoms. The *x*-axis is perpendicular to the *y*-axis, i.e. indicates the distance of the mobile proton to the N1···N3 axis. Proton positions outside the molecular plane were not taken into account. The potential energy surface of Fig. 11 was constructed using MOPAC version 6.0 as follows. We choose given values for the coordinates *x* and *y* for the mobile proton, and optimized the positions of the other protons and all heavy atoms, keeping both terminal nitrogen atoms on the *y*-axis. We note that this surface is a crude approximation, because not only the proton motion contributes to the reaction surface but also motions of the other atoms, in particular a rotation of trimethylamine around its molecular symmetry axis C_3 with respect to **1**. Although this rotation was not analyzed in detail, and is probably not very important, one can anticipate a hindered rotation depending on the proton position. If this rotation were not taken into account, the proton transfer would not be degenerate. Only half of the surface was calculated, the other half corresponds to the mirror image.

The energy surface obtained contained several stationary states. The dashed line on the left side of the energy surface of Fig. 11 illustrates the proton transfer pathway, the dashed line on the right side the pathway of the nitrogen atom N4 of trimethylamine. A and C correspond to the stable initial and final states which are degenerate, as we let the trimethylamine group readjust its rotational angle. B represents the saddle point for the base catalyzed reaction. D corresponds to a second saddle point where the mobile proton remains in the triazene. Both saddle points are separated by a barrier. We note that D is also present in the absence of the base. The energies of these stationary states are included in Fig. 11.

As the energy of B was about 6 times larger than the experimental energy of activation of 23 kJ mol^{-1} (Table 7) we performed additional calculations of the stationary points. Firstly, we recalculated their structures using PM3-MNDO version 7.0. The structures and energies obtained were essentially the same as those from version 6.0. The structures of A (C) and B obtained were then used as input parameters in order to calculate a more realistic energies using the quantum-mechanical ab initio program package Gaussian 03 [28]. In particular, the density functional theory method B3LYP (Becke 3-parameter Lee–Yang–Parr) was chosen using the 6-31G* basis set. Structures A (C) were completely relaxed. In the case of structure B, the coordinates of the proton in the bifurcated hydrogen bond were kept constant, whereas all other atoms were relaxed, and the structure optimized to the transition state. In order to improve the geometry convergence for B, force constants were evaluated at the starting geometry. The stationarity condition of all structures was verified by calculating the respective frequencies. No imaginary frequencies where observed in the case of A (C), whereas one imaginary frequency was calculated for the transition state B. Moreover, in order to take solvent effects into account for the discrepancy we used the polarized continuum solvent method and the self-consistent reaction field in Gaussian 03 for chloroform and for THF. Polarizability functions were used for the hydrogen atoms and for the heavy atoms, while diffusion functions were added only to the heavy atoms. The structures and energies obtained are depicted in Fig. 12.

While the fluorophenyl rings in the structures A (C) are almost located in the molecular plane, exhibiting only a twist angle of 0.1°, the rings are turned away in

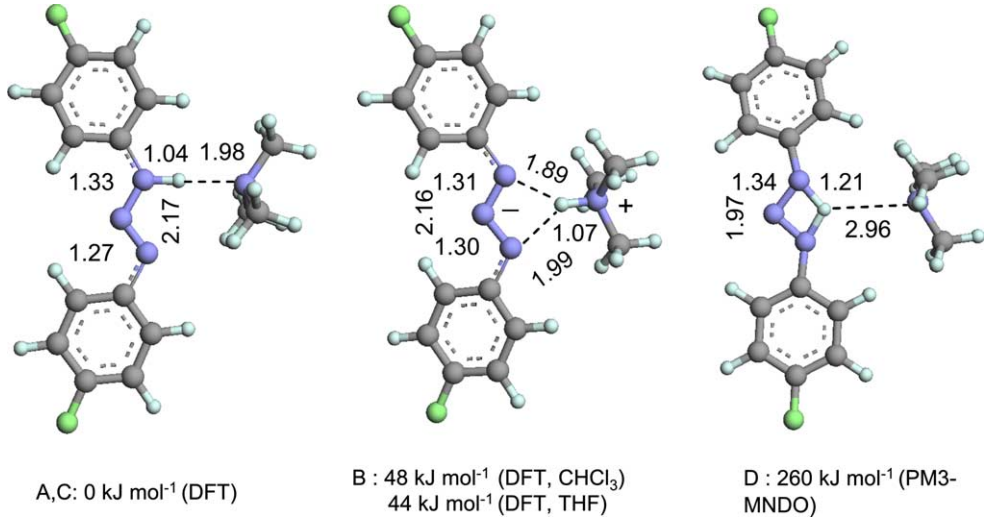

Fig. 12. Structures and energies of the stationary states of the surface of Fig. 11; A–C have been optimized using the DFT B3LYP method in Gaussian 03 [28], and single point energies have been calculated in solution with the PCM solvation model. Structure D is taken from the semi-empirical PM3 calculation using MOPAC 7.0 [27]. The distances are given in Å. Structures were drawn using ArgusLab 4.0 (Planaria Software LLC).

B from the plane of the triazene nitrogen atoms by −0.6° and 0.4°. This effect probably arises from an interference of the phenyl hydrogens with the base methyl groups during a twist of the base upon proton transfer.

The energy difference between A and B is 48 kJ mol^{-1} for chloroform and 44 kJ mol^{-1} for THF. These values represent still twice the experimental value of 23.2 kJ mol^{-1} and need to be further optimized in the future. Nevertheless, we do not expect major changes of the geometry of B when carrying out this procedure. The proton is almost completely transferred to the nitrogen atom of the base, resulting in a zwitterionic state. The NH-distance is found to be 1.07 Å, which is in good agreement with the value 1.075 Å of trimethylammonium chloride found by dipolar NMR [29]. B is then characterized by a bifurcated hydrogen bond to the terminal nitrogen atoms of **1** (1.89 and 1.99 Å, respectively), reinforced by the electrical charges. This Coulomb interaction prevents B from dissociation into the ions, in contrast to the initial states where only hydrogen bond interactions between **1** and the base prevail. B is substantially lower in energy than the second saddle point D. Its structure, calculated using PM3-MNDO MOPAC 7.0, is depicted in Fig. 11. The calculated energy of 260 kJ mol^{-1} was found to be larger than the value calculated with MOPAC 6.0. As this point could not be compared with the experiment, we did not further study the origin of this difference, nor tried to optimize this point using the DFT method. We note that Pye et al. [16] have calculated a value of 240 kJ mol^{-1} for this transition state for the unsubstituted triazene in the absence of the base. As the semi-empirical calculations normally yield energy values which are much larger than those obtained from ab initio methods it seems that the aryl groups stabilized state D.

The bifunctional proton exchange of **1** with **2** probably also occurs via protonation of the amine according to Scheme 2c, because the exchange with water is much slower. This points into the quantum-mechanical calculations of Pye et al. [16] who found that the exchange of water with unsubstituted triazene proceeds by protonation of the latter according to Scheme 2c.

5.4. Kinetic isotope effects: single vs. double barrier case

For the intramolecular single proton transfer of **1** catalyzed by trimethylamine **3** no kinetic H/D isotope effect was observed, with a tendency of even values smaller than unity. The corresponding reaction of **1** with **2** exhibited small effects of the order of 1.2. The kinetic HH/HD isotope effects observed for the bifunctional double proton transfer of **1** with **2** were found to be a little bit larger, typically about 1.7. These values are very small as compared to those obtained previously for other single [30] and double proton transfers [25b,8] in NHN-hydrogen bonded systems. The origin of kinetic H/D isotope effects is depicted schematically in Fig. 13. They arise when the zero-point energy difference ΔZPE of a given mobile proton site is decreased in the transition state and/or when the transfer occurs by tunneling.

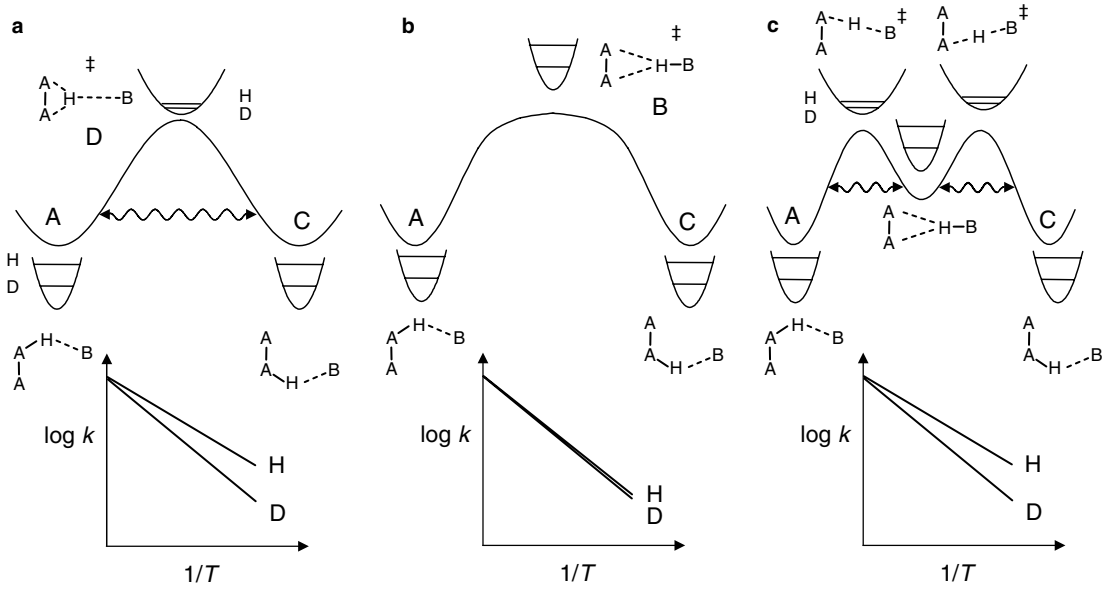

Fig. 13. Expected temperature-dependent kinetic H/D isotope effects of a degenerate base-catalyzed single proton transfer. (a) Single barrier or "concerted" case. (b) "Plateau-reaction" and (c) double barrier or stepwise case. The zero-point energies of H and D are visualized using the harmonic approximation. Tunneling between potential wells is visualized by sinusoidal arrows. Tunneling in (b) is absent because of major heavy atom motions implying large tunneling masses. For further explanations see text.

For the intramolecular base catalyzed reaction one can conceive a single-barrier case (Fig. 13(a)), a double barrier case (Fig. 13(c)) and intermediate case (Fig. 13(b)). In the single barrier case, the old and the new bond of the hydron transferred are both partially broken and formed. The hydrons transferred all loose substantial *ZPE* in the transition state, mainly because of a lowering of their zero-point energies [32]. This transition state may be identified with state D in Figs. 11 and 12. Large kinetic H/D isotope effects result for the over-barrier reaction according to Bigeleisen theory [33], as indicated by the Arrhenius curves included at the bottom of the figure, which are valid at high temperatures. At low temperatures, tunneling between the potential wells can dominate, as visualized by sinusoidal arrows. This can lead to larger isotope effects, but requires also little heavy atom motions which would lead to large tunneling masses and low tunneling probabilities. The "stepwise" mechanism involves two barriers and one intermediate, where the proton is transferred to the base. Here, also substantial kinetic H/D isotope effects are expected, arising from the over-barrier reactions and from tunneling. The intermediate case involves a very large barrier "plateau", where the center corresponds to transition state B of Figs. 11 and 12. In the plateau regime, the hydron is bound to the base, and exhibits, therefore, usual stretching and bending frequencies. This means that there is almost no change of the *ZPE* between the initial states A and C and the transition state B, and hence, only small kinetic isotope effects are expected at high temperatures. As the base has to be displaced during the reaction, and solvent reorganisation has to occur in the transition state, tunneling will be unlikely to occur because of very large tunneling masses.

The situation for the bifunctional base-catalyzed single barrier case is depicted in Fig. 14(a). Both protons loose zero-point energy in the transition state, mainly because of a lowering of their zero-point energies by hydrogen bond compression [32]. This situation is characterized at high temperatures by two large and similar HH/HD and HD/DD isotope effects, as indicated in the corresponding Arrhenius curves depicted below [31]. At low temperatures, tunneling can lead to concave Arrhenius curves and deviations from this "rule of the geometric mean". In Fig. 14c is depicted the double barrier or "stepwise" case which involves also substantial kinetic H/D isotope effects. Tunneling is hindered by the large energy of the intermediate. Finally, Fig. 14b represents an intermediate case involving again a barrier plateau. Double-proton transfer plateau reactions have been studied theoretically by Rauhut et al. [34]. However, multiple kinetic HH/HD/DD isotope effects have not yet been elucidated theoretically. However, some of us have argued some time ago that the kinetic HH/HD/DD isotope effects should be small, and the rule of geometric mean should be fulfilled as illustrated in the Arrhenius diagram of Fig. 14(b) [35], because both mobile protons will exhibit similar zero-point energies in both the initial and the transition states. This is indeed what is observed here for the reaction of **1** with **2**, which provides again evidence that the exchange is assisted by the basicity of **2**.

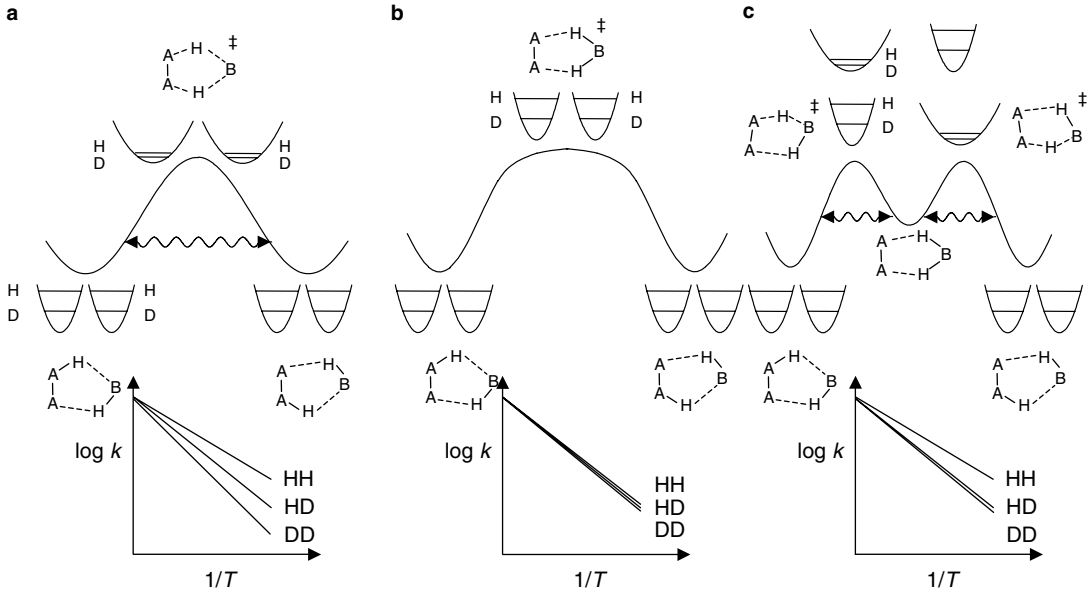

Fig. 14. Expected temperature dependent kinetic HH/HD/DD isotope effects of degenerate double proton transfers. (a) Single barrier or "concerted" case. (b) Plateau-reaction and (c) double barrier or stepwise case. For further explanations see Fig. 13 and text.

5.5. Catalyzed proton exchange reactions

We come back to the problem of the residual proton exchange of **1** via the structural decomposition isomer X = **4** because of its general importance for proton exchange studies by NMR. This is because among the many proton donors only very few of them exhibit the property of forming cyclic hydrogen bonded intermediates in which a multiple proton transfer can take place. In our laboratory, we had made great efforts in the past decade to find this kind of molecules. Most proton donors, however, exchange protons with the assistance of catalysts, which can either be an impurity of the donor itself or be introduced by the solvent or during the sample preparation process.

By NMR, the inverse life times or pseudo-first order rate constants τ_{AX}^{-1} of a proton donor A exchanging protons with a catalyst X according to Eq. (3) are measured. The values of τ_{AX}^{-1} depend on the concentrations of the partners, the equilibrium constant K of the formation of the reactive complex, and on the rate constant k_{AX} of the exchange in the reactive complex. Eq. (8) and Table 1 predict that τ_{AX}^{-1} decreases when the concentration of A is increased, and the concentration of X is constant, as one might expect for the case of a solvent impurity such as residual water. By contrast, when the concentration of X is related with the concentration of A, i.e. if $r = C_X/C_A$ is constant, a second-order rate law is obtained where $\tau_{AX}^{-1} = rk_{AX}KC_A$ when K is small, mimicking the reaction of two molecules of the type A in a cyclic dimer. On the other hand, when K is large, $\tau_{AX}^{-1} = rk_{AX}$, i.e. a rate law is obtained which is first order with respect to C_A.

With these results in mind, let us discuss the finding of either first- or second-order rate laws reported by Lunazzi et al. [12] for the proton self-exchange of diaryltriazenes. Formally, these findings are in agreement with the mechanism of Scheme 2a, assuming a large equilibrium constant K of the formation of cyclic dimers in case of the first order and a small constant in case of the second-order processes. However, this explanation is not satisfying because **1** and also other triazenes do not exhibit the low-field chemical shifts at increasing concentration found for the mobile protons of diarylamidines in tetrahydrofuran [9c], typical for the formation of the hydrogen bonded cyclic dimers which also prevail in the solid state [10]. Therefore, the explanation of second- or first-order rate laws of the triazene self-exchange in terms of an unidentified species is more likely, catalyzing the proton exchange according to Scheme 2c. Such a species could have been a rare conformer, for example an s-*cis* form, for which evidence was obtained here for the first time in the case of **1**. As indicated by the solid lines in Fig. 4, the second-order regime is realized at low concentrations or small equilibrium constants K of the formation of the reactive complex between the triazene and the catalytic species. In this case, however, reproducible rate constants will be obtained, in contrast to our finding for **1**; therefore, the catalytic species has to be here a decomposition product of **1**, probably of the structure **4**. This can explain, why the observed self-exchange rates of **1** vary from sample to sample. In case where the concentration of catalytic species is constant, arising for example from a constant solvent impurity such as water, the pseudo-first-order rate constants measured should decrease with increasing triazene concentration. The kinetics of the reaction of **1** with the unidentified catalytic impurity could not be followed because its concentration was unknown. Only, the energy of activation was determined to be around 17 kJ mol^{-1}; moreover, a kinetic HD/DD isotope effect of about 1.7 was observed, which is compatible with a double proton transfer according to Scheme 2c.

The reason why the proton exchange in cyclic hydrogen bonded dimers of diaryltriazenes is largely suppressed in contrast to the diarylformamidines was already rationalized in the introduction: the aryl groups are coplanar to the triazene unit, precluding the formation of such dimers with short N···N distances of about 3 Å [9d], whereas in the diarylamidines the approach is possible because the aryl rings are not coplanar with the amidine unit due to steric interactions of the aromatic protons and the formyl proton. This interpretation shows how important small changes of the chemical structure can be for the molecular function.

At this stage, we want to comment a result found by one of us concerning the proton exchange of malonaldehydedianil (or *N*-[3-(phenylamino)-2-propenylidene]-benzenamine) (**5**, Fig. 15) three decades ago which has been a mystery since this time [36]. This system was the first in a long series of dynamic NMR studies of proton transfer in our laboratory. According to Fig. 15(a), this molecule is present in CS_2 solution at room temperature as a *cis*-form characterized by an intramolecular hydrogen bond in which a fast intramolecular proton transfer takes place. At low temperatures, a *trans*-form was found which forms cyclic trimers, exhibiting a concerted triple proton transfer according to Fig. 15(b) which could be followed by dynamic NMR. The latter process involved a normal pre-exponential factor of the order of 10^{12} s^{-1}. However, the *cis*-form was subject to an intermolecular proton exchange, exhibiting a large negative entropy of activation but a first-order rate law. Although we have not re-studied this system here, we can now at least offer for the first time an explication: there had to be an unidentified species BH which catalyzes the proton exchange according to Fig. 15(a). The most likely molecule is a remaining *trans*-form, which finds as hydrogen bond partner only *cis*-molecules. The first-order rate law is again explained in terms of a large equilibrium constant for the formation of the reactive complex in which the exchange takes place.

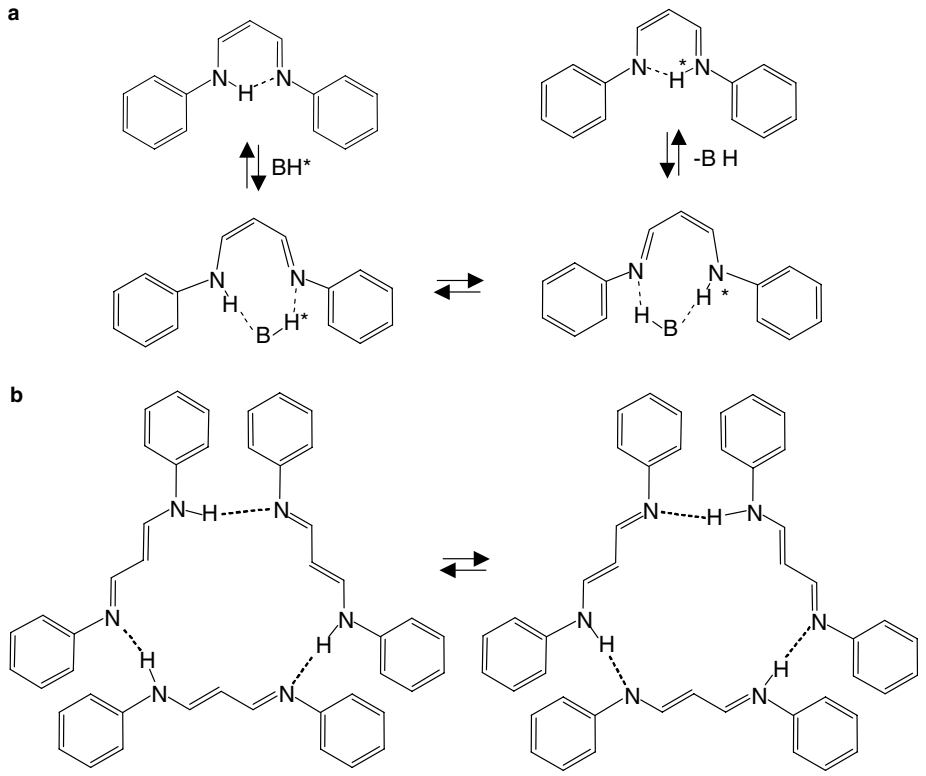

Fig. 15. Proton exchange of the monomeric *cis*-form (a) and of the trimeric *trans*-form (b) of malonaldehydedianil **5** studied in [36].

5.6. Hydrogen bond dynamics

As bifunctional double proton transfer has been assumed to be a more efficient process in aprotic environment for exchanging protons than a monofunctional catalysis [4,5] which generally requires the last dissociation step in Eq. (1) it was at first surprising for us that the intramolecular monofunctional proton transfer between **1** and **2** is faster than the intermolecular bifunctional transfer of the same molecules. The fast intramolecular transfer occurs, however, without dissociation, involving a hydrogen bond switch of the intermediate $A^{-}\cdots H\text{–}B^{+}$ according to Scheme 2b. This switch is faster than the dissociation process or the

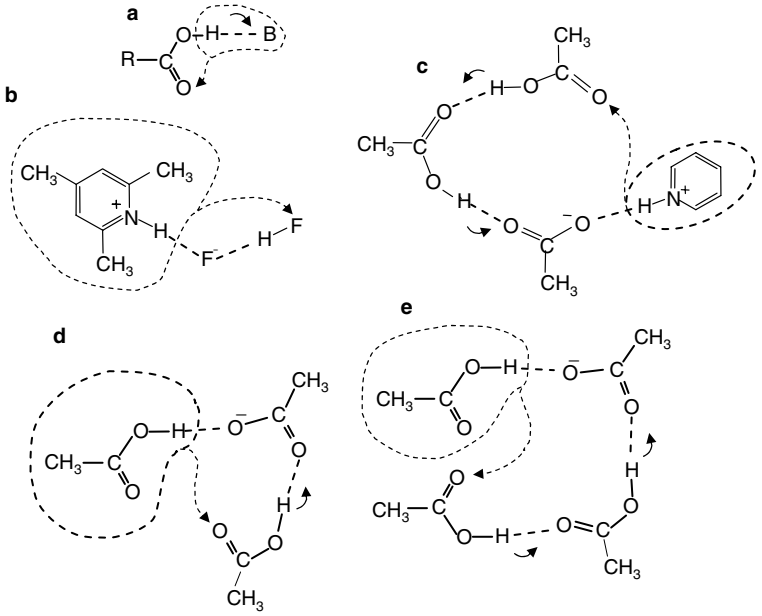

Scheme 3.

intermolecular bifunctional double proton transfer. This result is in agreement with the concept that hydrogen bonded complexes in aprotic environment are not static but fluxional, especially with respect to degenerate hydrogen bond switches. Here, the switch is monitored by the proton transfer coupled to the switch.

Some of us have obtained related fast hydrogen bond switches proceeding without dissociation hydrogen bonded complexes of acetate with acetic acid [37], pyridine with acetic acid [38], and of collidine with HF according to Scheme 3 [39]. In the latter case, the activation energy for the reorganization was also only about 20 kJ mol^{-1}. This research area is still unexplored, because these degenerate hydrogen bond switches can only be seen by NMR which needs to be done at very low temperatures and which requires suitable nuclear spin probes.

6. Conclusions

We have shown that *N*,*N*-diaryltriazenes are interesting model compounds for the study of intramolecular and intermolecular base-catalyzed proton transfer reactions. Interesting Arrhenius curves are obtained, exhibiting a convex curvature, which contrasts concave curvatures arising from tunneling. The convex curvature arises here from the fact, that the reactive complex in which the proton transfer takes place, dissociates at high temperatures.

The intramolecular base catalyzed transfer proceeds via a proton transfer to the base and an associated hydrogen bond switch. In the transition state, the proton is bound to the base, exhibiting a usual zero-point energy. This finding, as well as major motions of the base along a ''plateau'' preclude large kinetic H/D isotope effects. The process does not require dissociation into the free cation and the anion, which would involve a considerable free energy. It can, therefore, sometimes constitute an alternative mechanism to bifunctional intermolecular base catalysis [4,5]. This because the usual assumption that dissociation is required in a monofunctional base catalyzed process is not a pre-requisite in the monofunctional hydrogen-bond switch assisted catalytic process. Our results support especially the idea of the lysine amino group in enzymes as a proton carrier from one substrate site to another via a proton uptake, displacement of the ammonium group in space and subsequent proton release to another site of the substrate instead of a bifunctional proton transfer [5h]. Thus, in future computational and experimental studies of proton transfer pathways in functional proteins, we think it is worth also to explore the monofunctional pathway even if it requires major heavy atom motions.

Acknowledgments

This work was supported by the Deutsche Forschungsgemeinschaft, Bonn, the Russian Federation of Basic Research, Moscow, and the Fonds der Chemischen Industrie, Frankfurt.

References

[1] (a) J.P. Richard, Biochemistry 37 (1998) 4305;
(b) A.J. Kirby, Acc. Chem. Res. 30 (1997) 290;
(c) W.W. Cleland, P.A. Frey, J.A. Gerlt, J. Biol. Chem. 273 (1998) 25529;
(d) J.P. Guthrie, R. Kluger, J. Am. Chem. Soc. 115 (1993) 11569;
(e) K.B. Schowen, H.H. Limbach, G.S. Denisov, R.L. Schowen, Biochim. Biophys. Acta 1458 (2000) 43.
[2] (a) M.D. Toney, J.F. Kirsch, Biochemistry 32 (1993) 1471;
(b) X. Zhou, M.D. Toney, Biochemistry 38 (1998) 311.
[3] (a) H. Luecke, B.B. Schobert, H.T. Richter, J.P. Cartailler, J.K. Lanyi, J. Mol. Biol. 291 (1999) 899;
(b) H. Kandori, Y. Yamazaki, J. Sasaki, R. Needleman, J.K. Lanyi, A. Maeda, J. Am. Chem. Soc. 117 (1995) 2118.
[4] (a) C.G. Swain, J.F. Brown, J. Am. Chem. Soc. 74 (1952) 2534;
(b) C.G. Swain, J.F. Brown, J. Am. Chem. Soc. 74 (1952) 2538;
(c) M.M. Cox, W.P. Jencks, J. Am. Chem. Soc. 103 (1981) 580;
(d) W.P. Jencks, Chem. Soc. Rev. 10 (1981) 345;
(e) C.L. Perrin, R.E. Engler, D.B. Young, J. Am. Chem. Soc. 122 (2000) 4877;
(f) J.N. Roitenan, D.J. Cram, J. Am. Chem. Soc. 90 (1971) 2225;
(g) J.N. Roitenan, D.J. Cram, J. Am. Chem. Soc. 90 (1971) 2231;
(h) R.P. Bell, J.E. Critchlow, Proc. R. Soc. London, Ser. A (1971) 325;
(i) A.M. Klaer, H. Nielsen, P.E. Sorenson, J. Ulstrup, Acta Chem. Scand. A34 (1980) 281.
[5] (a) M. Ek, P. Ahlberg, Chem. Scripta 16 (1980) 62;
(b) K.A. Engdahl, H. Bivehed, P. Ahlberg, W.H. Saunders Jr., J. Chem. Soc., Chem. Commun. (1982) 423;
(c) M. Ek, P. Ahlberg, Acta Chem. Scand. B38 (1984) 211;
(d) P. Ahlberg, K. Janné, S. Löfås, F. Nettelblad, L. Swahn, J. Phys. Org. Chem. 2 (1989) 429;
(e) Y.K. Wu, P. Ahlberg, Acta Chem. Scand. 46 (1992) 60;
(f) Y.K. Wu, P. Ahlberg, J. Org. Chem. 57 (1992) 6324;
(g) U. Berg, N. Bladh, Acta Chem. Scand. 51 (1997) 778;
(h) A. Hjelmencrantz, U. Berg, J. Org. Chem. 67 (2002) 3585.
[6] (a) B.H. Meier, F. Graf, R.R. Ernst, J. Chem. Phys. 76 (1982) 768;
(b) R. Meyer, R.R. Ernst, J. Chem. Phys. 93 (1990) 768;
(c) A. Heuer, U. Haeberlen, J. Chem. Phys. 95 (1991) 4201;
(d) A. Stöckli, B.H. Meier, R. Kreis, R. Meyer, R.R. Ernst, J. Chem. Phys. 93 (1990) 1502;
(e) A.J. Horsewill, D.F. Brougham, R.I. Jenkinson, C.J. McGloin, H.P. Trommsdorff, M.R. Johnson, Ber. Bunsen. Phys. Chem. 102 (1998) 317;
(f) M.A. Neumann, S. Craciun, A. Corval, M.R. Johnson, A.J. Horsewill, V.A. Benderskii, H.P. Trommsdorff, Ber. Bunsen. Phys. Chem. 102 (1998) 325;
(g) T. Loerting, K.R. Liedl, J. Am. Chem. Soc. 120 (1998) 12595.
[7] (a) D. Gerritzen, H.H. Limbach, J. Am. Chem. Soc. 106 (1984) 869;
(b) A. Fernández-Ramos, Z. Smedarchina, J. Rodríguez-Otero, J. Chem. Phys. 114 (2001) 1567.
[8] (a) F. Aguilar-Parrilla, O. Klein, J. Elguero, H.H. Limbach, Ber. Bunsen. Phys. Chem. 101 (1997) 889;

(b) O. Klein, M.M. Bonvehi, F. Aguilar-Parrilla, J. Elguero, H.H. Limbach, Israel J. Chem. 34 (1999) 291;
(c) O. Klein, F. Aguilar-Parrilla, J.M. Lopez, N. Jagerovic, J. Elguero, H.H. Limbach, J. Am. Chem. Soc. 126 (2004) 11718.
[9] (a) L. Meschede, D. Gerritzen, H.H. Limbach, Ber. Bunsen. Phys. Chem. 92 (1988) 469;
(b) H.H. Limbach, L. Meschede, G. Scherer, Z. Naturforsch. 44a (1989) 459;
(c) L. Meschede, H.H. Limbach, J. Phys. Chem. 95 (1991) 10267;
(d) R. Anulewicz, I. Wawer, T.M. Krygowski, F. Männle, H.H. Limbach, J. Am. Chem. Soc. 119 (1997) 12223.
[10] R. Anulewicz, Acta Crystallogr. C53 (1997) 345.
[11] A.N. Nesmeyanov, E.V. Borisov, D.N. Kravtsov, A.S. Peregudov, E.I. Fedin, Izv. Akad. Nauk SSSR Ser. Khim. (1981) 110.
[12] L. Lunazzi, G. Panciera, J. Chem. Soc., Perkin 2 (1980) 52.
[13] J. Benes, V. Beranek, J. Zimprich, P. Vetesnik, Collect. Czech., Chem. Commun. (Engl.) 42 (1977) 702.
[14] J. Baro, D. Dudek, K. Luther, J. Troe, Ber. Bunsen. Phys. Chem. 87 (1983) 1155, 1161.
[15] F. Männle, H.H. Limbach, Angew. Chem., Int. Ed. Engl. 35 (1996) 441.
[16] C.C. Pye, K. Vaughan, J.F. Glister, Can. J. Chem. 80 (2002) 447.
[17] D.G. Truhlar, A. Kohen, Proc. Natl. Acad. Sci. 98 (2001) 848.
[18] T. Axenrod, P.S. Pregosin, M.J. Wieder, E.D. Becker, R.B. Bradley, G.W.A. Milne, J. Am. Chem. Soc. 93 (1971) 6536.
[19] D.G. Ott, Synthesis with Stable Isotopes, New York, 1981.
[20] G. Hartmann, R. Dickey, Organic Synthesis, Coll. vol. II, Wiley, New York, 1943, p. 163.
[21] H.H. Limbach, Dynamic NMR spectroscopy in the presence of kinetic hydrogen/deuterium isotope effects, in: NMR Basic Principles and Progress. Deuterium and Shift Calculation, vol. 23, Springer-Verlag, Heidelberg, 1991, pp. 66–167.
[22] M. Eigen, Angew. Chem., Int. Ed. Engl. 3 (1964) 1.
[23] J.C. Scaiano, C.P. Chen, Mc P.F. Garry, J. Photochem. Photobiol. A: Chem. 62 (1991) 75.
[24] J. Hennig, H.H. Limbach, J. Magn. Reson. 49 (1982) 322.
[25] (a) E.F. Caldin, S. Mateo, J. Chem. Soc., Faraday Trans. I 71 (1975) 1876;
(b) G. Scherer, H.H. Limbach, J. Am. Chem. Soc. 116 (1994) 1230.
[26] A. Kohen, R. Cannio, S. Bartolucci, J.P. Klinman, Nature 399 (1999) 496.
[27] (a) J.J.P. Stewart, J. Comput. Chem. 10 (1989) 209, 221;
(b) J.J.P. Stewart, MOPAC 6.0 and 7.0, A Semi-Empirical Molecular Orbital Program, Quantum Chemistry Program Exchange, Indiana University, Bloomington, #455, http://qcpe.chem.indiana.edu/.
[28] M.J. Frisch, G.W. Trucks, H.B. Schlegel, G.E. Scuseria, M.A. Robb, J.R. Cheeseman, J.A. Montgomery Jr., T. Vreven, K.N. Kudin, J.C. Burant, J.M. Millam, S.S. Iyengar, J. Tomasi, V. Barone, B. Mennucci, M. Cossi, G. Scalmani, N. Rega, G.A. Petersson, H. Nakatsuji, M. Hada, M. Ehara, K. Toyota, R. Fukuda, J. Hasegawa, M. Ishida, T. Nakajima, Y. Honda, O. Kitao, H. Nakai, M. Klene, X. Li, J.E. Knox, H.P. Hratchian, J.B. Cross, C. Adamo, J. Jaramillo, R. Gomperts, R.E. Stratmann, O. Yazyev, A.J. Austin, R. Cammi, C. Pomelli, J.W. Ochterski, P.Y. Ayala, K. Morokuma, G.A. Voth, P. Salvador, J.J. Dannenberg, V.G. Zakrzewski, S. Dapprich, A.D. Daniels, M.C. Strain, O. Farkas, D.K. Malick, A.D. Rabuck, K. Raghavachari, J.B. Foresman, J.V. Ortiz, Q. Cui, A.G. Baboul, S. Clifford, J. Cioslowski, B.B. Stefanov, G. Liu, A. Liashenko, P. Piskorz, I. Komaromi, R.L. Martin, D.J. Fox, T. Keith, M.A. Al-Laham, C.Y. Peng, A. Nanayakkara, M. Challacombe, P.M.W. Gill, B. Johnson, W. Chen, M.W. Wong, C. Gonzalez, J.A. Pople, Gaussian 03, Revision B.04, Gaussian, Inc., Pittsburgh, PA, 2003.
[29] C.G. Hoelger, H.H. Limbach, J. Phys. Chem. 98 (1994) 11803.
[30] (a) J. Braun, M. Schlabach, B. Wehrle, M. Köcher, E. Vogel, H.H. Limbach, J. Am. Chem. Soc. 116 (1994) 6593;
(b) J. Braun, R. Schwesinger, P.G. Williams, H. Morimoto, D.E. Wemmer, H.H. Limbach, J. Am. Chem. Soc. 118 (1996) 11101, and papers cited therein.
[31] H.H. Limbach, O. Klein, J.M. Lopez, J. Elguero, Z. Phys. Chem. 217 (2004) 17.
[32] S.N. Smirnov, H. Benedict, N.S. Golubev, G.S. Denisov, M.M. Kreevoy, R.L. Schowen, H.H. Limbach, Can. J. Chem. 77 (1999) 943.
[33] (a) J. Bigeleisen, J. Chem. Phys. 17 (1949) 675;
(b) J. Bigeleisen, J. Chem. Phys. 23 (1955) 2264;
See also L. Melander, W.H. Saunders, Reaction Rates of Isotopic Molecules, Krieger, Malabar, FL, 1987.
[34] (a) S. Schweiger, G. Rauhut, J. Phys. Chem. A 107 (2003) 9668;
(b) S. Schweiger, B. Hartke, G. Rauhut, Phys. Chem. Chem. Phys. 6 (2004) 3341;
(c) S. Schweiger, B. Hartke, G. Rauhut, Phys. Chem. Chem. Phys. 7 (2005) 493.
[35] H. Rumpel, H.H. Limbach, J. Am. Chem. Soc. 111 (1989) 5429.
[36] (a) H.H. Limbach, W. Seiffert, Ber. Bunsen. Phys. Chem. 78 (1974) 532;
(b) H.H. Limbach, W. Seiffert, Ber. Bunsen. Phys. Chem. 78 (1974) 641.
[37] P.M. Tolstoy, P. Schah-Mohammedi, S.N. Smirnov, N.S. Golubev, G.S. Denisov, H.H. Limbach, J. Am. Chem. Soc. 126 (2004) 5621.
[38] S.N. Smirnov, N.S. Golubev, G.S. Denisov, H. Benedict, P. Schah-Mohammedi, H.H. Limbach, J. Am. Chem. Soc. 118 (1996) 4094.
[39] I.G. Shenderovich, P.M. Tolstoy, N.S. Golubev, S.N. Smirnov, G.S. Denisov, H.H. Limbach, J. Am. Chem. Soc. 125 (2003) 11710.